Die approbierte Originalversion dieser Diplom-/Masterarbeit ist in der Hauptbibliothek der Technischen Universität Wien aufgestellt und zugänglich.
http://www.ub.tuwien.ac.at
The approved original version of this diploma or master thesis is available at the main library of the Vienna University of Technology.
http://www.ub.tuwien.ac.at/eng

TECHNISCHE UNIVERSITÄT WIEN
Vienna University of Technology

DIPLOMARBEIT

Characterization and preparation of thermoluminescence dosimeters for surface and in vivo dose measurements

AUSGEFÜHRT AM

Atominstitut
Fakultät für Physik
Technische Universität Wien

IN ZUSAMMENARBEIT MIT DER

Universitätsklinik für Strahlentherapie
Medizinische Universität Wien

UNTER DER ANLEITUNG VON

Univ.Prof. Dipl.-Ing. Dr. Dietmar Georg
und
Dr. Monika Clausen

EINGEREICHT VON

Adrian Thummerer
Sonnenstraße 6
3340 Waidhofen an der Ybbs

Contents

Acknowledgement

First of all, I would like to thank Prof. Dr. Dietmar Georg for supervising this thesis and giving me the opportunity to work on my master thesis in the Department of Radiotherapy at the Medical University of Vienna.

Further I wish to thank all people i had the chance to work with at MedAustron. It was an ideal environment for me to learn and work on this thesis. In particular, I would like to thank Dr. Monika Clausen for guiding me through every aspect of this work. Especially the support during writing this thesis is gratefully acknowledged.

Additionally, I would like to thank Barbara Knäusl, PhD and Mag. Peter Kuess, PhD for taking care of all organizational issues and providing help no matter what the problem was.

Moreover, I also want to thank my family for their support during this work and my entire studies.

Abstract

Due to their size, reusability and good accuracy thermoluminescent dosimeters (TLDs), are a valuable tool in radiation dosimetry. The properties of TLDs allow a convenient use in radiotherapy and radiation oncology not only for measurements in different types of phantoms but also for in-vivo dosimetry. The relatively small detectors can be conveniently placed in cavities and/or on surfaces to measure skin dose or dose close to organs at risk. This can help to verify treatment delivery. For future use of thermoluminescent detectors at MedAustron, the center for ion therapy and research in Wiener Neustadt, a set of TLD-100 detectors (LiF:Mg,Ti) was characterized and initial measurements were performed for use of TLDs in in-vivo and surface dose measurements.

The sample-to-sample uniformity of TLDs was verified to be within the limits stated by the manufacturer. Individual sensitivity factors for TLDs were determined and the reproducibility limits, given by the manufacturer were fulfilled by most of the investigated TLDs. Furthermore TLDs were calibrated in ^{60}Co and proton beams, where supralinearity was observed for both radiation types starting at the dose level of about 1 Gy. Individual sensitivity factors were applied to correct for varying sensitivity of TLDs. This reduced the standard deviation of measurements by 50 %. To investigate the response of thermoluminescent detectors in changing LET conditions, detectors were placed at several depths of a spread-out Bragg peak. The positioning of TLDs in multiple depths, without mutual shielding, was realized with in-house modified RW3 slabs. TLD results were compared to the response of radiochromic films, i.e. type EBT-3 and EBT-XD. For TLDs no quenching was observed in the investigated region of a spread-out Bragg peak while for EBT-3 and EBT-XD films the known LET dependence was confirmed.

The investigated TLDs, corrected with corresponding sensitivity factors, had proven to be well suited for clinical applications. Nevertheless, the consistency in the process of using and treating TLDs is a very crucial aspect. In order to maintain the good outcome, regular quality assurance of all involved parts is strongly recommended.

Zusammenfassung

Aufgrund ihrer kleinen Abmessungen, ihrer Wiederverwendbarkeit und ihrer guten Messgenauigkeit werden Thermolumineszenzdosimeter (TLDs) in vielen Bereichen als Strahlungsdetektor verwendet. In der Strahlentherapie bzw. Radioonkologie können TLDs nicht nur in einer Vielzahl an Phantomen sondern auch im Bereich der In-vivo-Dosimetrie eingesetzt werden. Aufgrund der kleinen Abmessungen können die Detektoren einfach an der Haut oder in Körperhöhlen (z.B Mundhöhle) befestigt werden. Für die Verwendung von Thermolumineszenzdetektoren bei MedAustron, Zentrum für Ionentherapie und Forschung, wurde ein Set von TLD-100 Detektoren charakterisiert und vorbereitende Messungen für den Einsatz von TLDs als Oberflächen- und In-vivo-Dosimeter durchgeführt.

Individuelle Sensitivitätsfaktoren wurden bestimmt, um die vom Hersteller angegebenen Eigenschaften der Detektoren zu überprüfen. Die Variation in einem Set von 48 TLD-100 Detektoren (< 15 %) und die Reproduzierbarkeit von einzelnen Dosimetern (< 2 %) überstieg die angegeben Werte nicht. Weiters wurden Thermolumineszenzdosimeter in ^{60}Co und Protonenstrahlung kalibriert. Die für auf Lithium-Fluorid basierende TLDs typische Supralinearität konnte für beide Strahlungsarten bei einem Dosislevel von ca. 1 Gy festgestellt werden. Durch die Korrektur mit Hilfe der individuellen Sensitivitätsfaktoren reduzierte sich die Standardabweichung bei Messungen mit Thermolumineszenzdosimeter um 50 %. Um das Verhalten in verschiedenen LET-Bedingungen zu testen, wurden TLDs in verschiedenen Tiefen eines modulierten Bragg-Peaks positioniert. Ein gegenseitiges Abschirmen wurde durch die Verwendung von hausintern angepassten RW3-platten verhindert. Radiochromfilme, vom Typ EBT-3 und EBT-XD, wurden zum Vergleich in den selben Tiefen bestrahlt und ausgewertet. Für TLDs wurde kein LET-Einfluss in modulierten Bragg-Peaks festgestellt werden. Für Filme hingegen konnte die bekannte LET-Abhängigkeit bestätigt werden.

Die durchgeführten Messungen belegen die Eignung von Thermolumineszenzdetektoren für klinische Anwendungen in Oberflächen und In-vivo-Dosimetrie. Die Beständigkeit des gesamten Thermolumineszenzprozesses (Ausheizen und Auslesen) ist von äußerster Wichtigkeit um präzise Resultate zu erzielen. Die regelmäßige Überprüfung und Wartung aller involvierten Geräte ist daher zu empfehlen.

1 Introduction

This chapter provides a brief overview about radiotherapy in general and focuses on particle therapy and the underlying physical principles. Furthermore detectors used in particle therapy, with a main focus on thermoluminescent detectors will be presented. At the end the MedAustron particle therapy facility will be briefly described.

1.1 Basics of radiotherapy

The treatment of a disease utilizing ionizing radiation is called radiotherapy. Depending on the position of a radiation source in relation to the patient, radiotherapy can be divided into following three types:

- external beam radiotherapy or teletherapy
- brachyterapy or sealed source radiotherapy
- unsealed source radiotherapy

In external beam radiotherapy (EBRT) the radiation is coming from a source that is located outside the patient whereas in brachytherapy a sealed radiation source is placed inside or around a tumor. In unsealed source radiotherapy radoopharmaceuticals are administered to the patient via ingestion or injection. Common radioactive sources in brachytherapy are ^{131}Cs, ^{137}Cs, ^{60}Co and ^{192}Ir, in unsealed source radiotherapy ^{131}I.

Photons are the most commonly used radiation type in EBRT. For clinical purpose energies ranging from 200 kV up to 25 MV are used. They can be either produced in conventional X-ray-tubes, in linear accelerators (LINAC) or are emitted by radioisotopes like ^{60}Co. Today in most cases LINACs are used because of their versatile, accurate and effective photon beam. They accelerate electrons towards a metal target and the loss in kinetic energy when hitting the target, results in the emission of Bremsstrahlung, which is than used for patient treatment. The depth-dose profile of photons is characterised by an initial build up to a maximum value followed by an exponential decrease (Fig. 1.1).

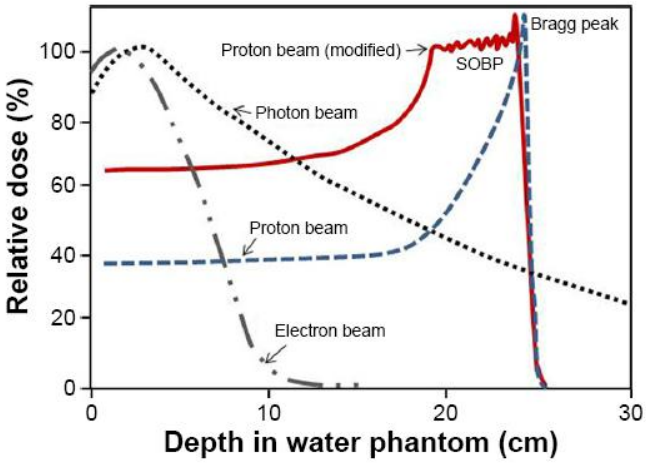

Fig. 1.1: Depth-dose profile for photons, electrons and protons (source [1]).

Beside photon beams also charged particle beams are used in external beam radiotherapy. In electron beams the depth dose profile shows a small initial build up region and a steep dose fall of after the maximum (Fig. 1.1). This makes electron beams beneficial for treatment of superficial tumors or during surgery (intra-operative electron radiotherapy). The depth dose profile of heavy charged particles (protons and ions) allow the treatment of profound tumors and at the same time sparing surrounding tissue. Heavy charged particle EBRT is discussed in more detail in the following section.

1.2 Particle therapy

Charged particles, like protons or ions, have, compared to photons and electrons, different dosimetric properties. The deposited dose of charged particles increases slowly with increasing depth. This results in the maximum dose deposited in the region of the Bragg peak, near the end of the range of a particle beam. This maximum is followed by a very sharp fall-off (see Fig. 1.1). When comparing the depth-dose profiles of photon and particle beams, the major advantage of particle beams is obvious. Due to the Bragg peak and the rapid drop behind it, higher dose can be delivered to a tumor while the surrounding healthy tissue, especially behind the tumor, is spared. The dimensions of a target are typically larger than the width of an unmodulated (pristine) Bragg peak and a superposition of Bragg peaks with varying energy and intensity is used. This creates an extended region of uniform dose which is called spread-out Bragg peak (SOBP). The characteristics of particle beams are especially advantageous for tumors close to organs at risk and pediatric patients, where the overall dose has to be kept as small as possible.

In the following sections physical basics of particle therapy are discussed.

1.2.1 Interaction of charged particles with matter

When a charged particle, surrounded by its Coulomb field, traverses an absorbing medium, it can either interact with orbital electrons or with nuclei of the absorbing medium. Deflection of the incident direction can happen through inelastic or elastic scattering and particles can loose kinetic energy via collisions (collision loss) or energy transfer to photons (radiation loss). The collision loss is mainly due to inelastic coulomb interactions with the orbital electrons while radiation loss arises from interaction with the Coulomb field of a nucleus. In individual interactions the traversing particle looses only a small fraction of its energy, hence a large number is necessary to stop a particle completely. The linear stopping power, $-dE/dx$, describes the energy loss per unit of path length in an absorbing medium. Dividing it by the density of the absorber gives the mass stopping power S. The mass stopping power S can be split into two contributions: radiation stopping power, also called nuclear stopping power, S_{rad} and collision stopping power, known as ionization or electronic stopping power, S_{col} [2].

$$S = -\frac{1}{\rho}\frac{dE}{dx} = S_{rad} + S_{col} \tag{1.1}$$

Radiation stopping, as result from interaction with nuclei of an absorber, is mainly experienced by light charged particles (electrons and positrons) and is negligible for heavy charged particles used in particle therapy. The collision loss is experienced by both, light and heavy charged particles, and leads to excitation and ionization of atoms in the traversed material [2].

The collision stopping power of heavy charged particles was first theoretically described in 1913 by Niels Bohr. In 1930 Bethe improved the theory by using relativistic and quantum mechanical concepts. At very low energies and relativistic energies Bethe's equation was not agreeing with experimental findings. Corrections to the original equation were contributed by Felix Bloch, Walter H. Barkas and Ugo Fano to reach better agreement over all energies. With this corrections the full equation can be written as [2]:

$$S_{col} = 4\pi\frac{N_A}{A}\left(\frac{e^2}{4\pi\epsilon_0}\right)^2\frac{z^2}{m_e c^2\beta^2}Z\left\{ln\frac{2m_e c^2}{I} + ln\frac{\beta^2}{1-\beta^2} - \beta^2 - \frac{C}{Z} - \delta\right\}, \tag{1.2}$$

where

Na = Avogadros number

A = atomic mass of absorbing material

e = elementary charge

ϵ_0 = vacuum permittivity

z = charge of particle in units of e

m_e = electron rest mass

c = speed of light

$\beta = \frac{v}{c}$

v = particle velocity

Z = atomic number of absorbing material

I = mean excitation potential

C = shell correction

δ = density correction

The above equation leads to the stopping power curve shown in Figure 1.2. The curve can be divided into three regions. The stopping power rises with increasing energy until a maximum is reached (region 1). From this maximum the stopping power decrease with $1/E$ until a minimum value is reached (2). At relativistic energies S_{col} rises slowly with increasing energy (3).

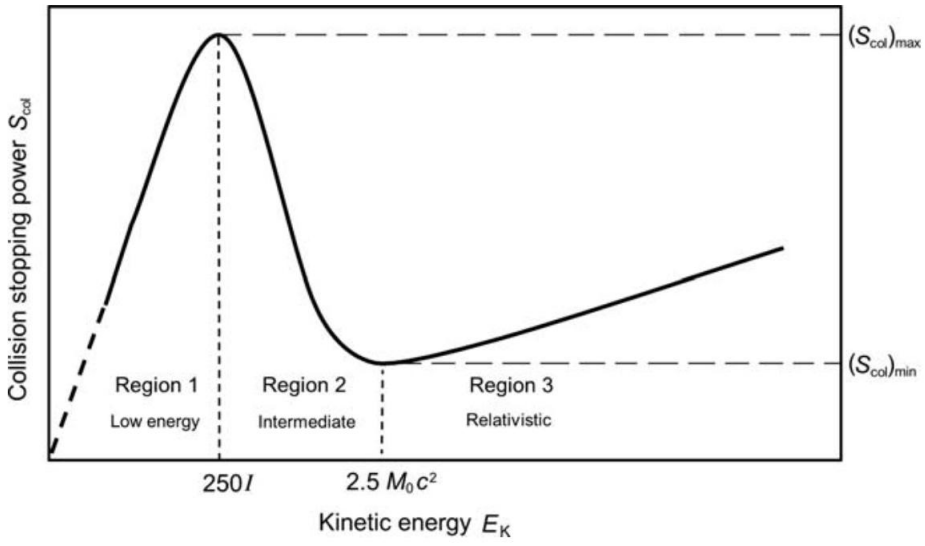

Fig. 1.2: Stopping power of heavy charged particles plotted against energy (source: [2]).

For energies used in particle therapy the stopping power increases with particles slowing down. This is responsible for the shape of the depth-dose profile and is hence the reason for the beneficial characteristics concerning radiotherapy.

1.2.2 Range of charged particles

In every individual collision heavy charged particles transfer only a small amount of their energy and suffer only small angle deflection through inelastic collisions. This results in an almost straight path when traversing a material. Light charged particles in contrast can loose up to half of their energy in a single collision and suffer large angle scattering which can lead to a twisted path.

The statistical nature of the energy loss process leads to a varying range for individual particles in a particle beam and is called range straggling. It's among other things responsible for the widening of the Bragg peak, since not all particles stop at the exact same depth. Different types and definitions of range are in use, some common ones are given below.

Path length: The path length is the total distance along a particles actual trajectory until it comes to rest, regardless of the direction of motion.

Projected range: The projected range is the sum of individual path lengths projected onto the incident particle direction.

CSDA range: Particles moving through a medium loose their energy in a high number of interactions. To simplify this the 'continuous slowing down approximation' (CSDA) assumes that the energy loss is not fractionated but happening continuously. This means the range can be calculated via:

$$R_{CSDA} = \int_0^{E_0} \frac{dE}{S(E)} \tag{1.3}$$

where R_{CSDA} is the CSDA range, E_0 is the initial kinetic energy and $S(E)$ is the mass stopping power.

Residual range: Residual range is defined as:

$$R_{res} = R_p - z \tag{1.4}$$

where z is the measurement depth and R_p the practical range, which is defined as the depth

behind a BP or SOBP where the dose has decreased to 10 % of the maximum value [3].

1.2.3 Multiple Coulomb scattering

Scattering of charged particles at the atomic nucleus lead to small angle deflections of their path. This happens multiple times while a charged particle is traversing matter and results in a net deflection (see Fig. 1.3). Because of the much higher mass of a charged particle, interactions with electrons do not lead to a noticeable deflection. The small but non-negligible deflections through multiple Coulomb scattering play a key role for the lateral profile of a particle beam.

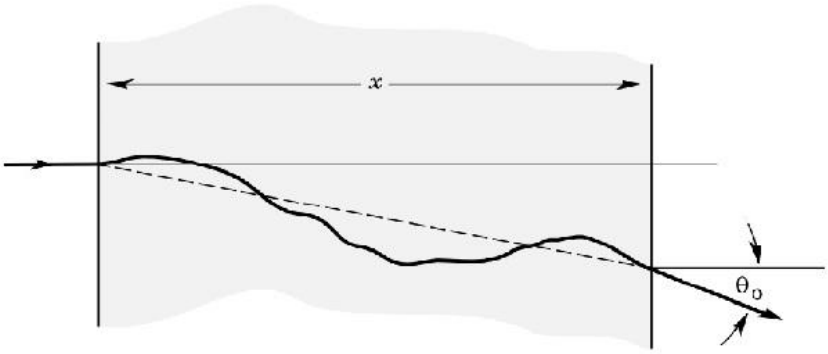

Fig. 1.3: Illustration of multiple Coulomb scattering (MCS) with many small angle deflections (source: [4])

1.2.4 Water equivalent depth (WED)

In terms of energy loss and nuclear interactions, water is very similar to human tissues and is therefore used as phantom material to measure depth and dose. The term of water-equivalent depth (WED) or thickness (WET) is often used to specify range of a proton beams in a certain material in relation to water. For example the WET of PMMA, frequently used as a phantom material, is 1.16 mm, which means that a beam traversing 1mm of PMMA would loose the same amount of energy traversing 1.16 mm of water [5, 6].

1.2.5 Linear energy transfer (LET)

The linear energy transfer (LET) is defined as

$$L_\Delta = \left.\frac{d\epsilon}{dl}\right|_\Delta \tag{1.5}$$

where $d\epsilon$ is the average energy locally imparted to a medium by a particle of a specified energy while traversing a distance dl [7]. The locality of the energy transfer is described by the subscript Δ, which defines the cutoff limit for the energy of secondary electrons. The L_∞, called unrestricted LET, is equal to the collision stopping power S_{col}, since all energy transfer events are included. In particle therapy the concept of LET is not only important because it quantifies the radiation quality but also biological impact of radiation on human tissue. Some detectors (e.g. film, TLDs) also show LET dependent response. This has to be considered accordingly when such detectors are chosen for use in particle beams.

1.3 Dosimetry in particle therapy

Radiation dosimetry is the measurement or computation of the quantity and quality of ionizing radiation. The basic physical quantity that is measured by detectors used in dosimetry is absorbed dose, defined as energy per unit mass absorbed by a medium. The unit of absorbed dose is the Gray (1 Gy = 1 J/kg). In radiotherapy the main interest lies in absorbed dose to water, since the human body consist mostly of water [8].

Radiation dosimetry systems, consisting of detector (dosimeter) and reader, can be divided into two types: absolute and relative. Absolute dosimetry systems have the ability to measure dose without a calibration in a known radiation field [9]. Used absolute radiation dosimetry systems are:

- **Calorimetric dosimetry system:** Thermal energy (heat), that is created by interaction of ionizing radiation with a material, is measured to quantify absorbed dose.
- **Chemical (Fricke) dosimetry system:** Chemical dosimetry is based on the quantification of reaction products which are produced by ionizing radiation interacting with radiation sensitive chemicals. Fricke dosimetry utilizes radiolysis of water and ferrous sulfate. The energy balance of the chemical reactions are well characterized and hence Fricke dosimetry can be used as absolute dosimetry system.
- **Ionometric dosimetry system:** Ionometric radiation dosimeters quantify the number of ions that are produced by ionizing radiation when traversing a medium (most commonly gas).

In radiotherapy the available absolute dosimetry systems are impractical for use in routine mea-

surements. Instead ionization chambers, calibrated in standard laboratories are good alternative for absolute dose measurements in radiotherapy. The calibration process for ionization chambers in particle beams is described in the following section.

Relative radiation dosimetry systems need to be calibrated in a known radiation field to give accurate information about absorbed dose. Common relative radiation dosimetry systems include radiographic film and thermoluminescence dosimeters. Ionization chambers can be used as absolute and relative radiation dosimeters.

A dosimetry system where the connection between reader and dosimeter is established and the signal is obtained during irradiation (e.g. ionization chamber) is called active. Whereas in passive detector systems the dosimeter accumulates a signal which is measured by the reader only after the irradiation (e.g TLDs, films) [9].

In general every material or setup, in which radiation creates a measurable signal, can be used as radiation detector. In radiotherapy dosimeters are needed to ensure that prescribed doses are accurately delivered to patients. Several stages including equipment testing, equipment or beam commissioning, calibration, treatment verification and quality assurance procedures require reliable detectors. A wide range of detectors has been developed and is available for these purposes [7, 10]. Some of the most frequently used detectors used in particle therapy are briefly described below. Thermoluminescent dosimeters are discussed in more detail in section 2.3.3.

1.3.1 Ionization chambers

Ionization chambers are gas filled detectors which measure ionizing radiation by collecting charges that are produced by ionizing radiation. Because of their convenient use and availability in many different sizes and shapes, ionization chambers have been adapted as standard dosimeter in (particle) radiotherapy. Ionization chambers are, despite the possibility to do so, not used as absolute dosimeters in radiotherapy. For absolute measurements the chamber volume and geometry has to be measured directly. This is challenging and is commonly not done. Instead ionization chambers are mainly calibrated in a known radiation field and used as relative dosimeter in radiotherapy. Concerning particle therapy, calibration in particle beams would be ideal, but these beams are not yet available in standard calibration laboratories. Therefore the calibration is performed in a different radiation quality (usually ^{60}Co) [8, 11]. A beam quality correction factor is than used to account for different beam quality.

The dose to water $D_{w,Q}$ in a proton beam with beam quality Q under reference conditions is than calculated via:

$$D_{w,Q} = M_Q N_{D,w,Q_0} k_{Q,Q_0} \,, \tag{1.6}$$

where M_Q is the reading of the dosimeter, N_{D,w,Q_0} the calibration factor for the calibration radiation quality Q_0 in terms of dose to water and k_{Q,Q_0} is a chamber specific factor that corrects for the difference of actual beam quality Q and calibration beam quality Q_0.

Ionization chambers are typically not used under reference conditions and appropriate correction factors have to be applied.

- **Temperature and pressure:** If pressure or temperature is different than the reference conditions (20°C and 101.3 kPa) k_{TP} has to be applied to correct the measured value. k_{TP} is defined as:

$$k_{TP} = \frac{273.2 + T}{273.2 + T_0} \frac{P_0}{P} \tag{1.7}$$

  Where T/P is the actual temperature/pressure and T_0/P_0 is the value at reference conditions.

- **Electrometer:** A electrometer correction factor k_{elec} has to be applied if electrometer and ionization chamber were calibrated separately. In case of a combined calibration of ionization chamber and electrometer this factor is already part of N_{D,w,Q_0} and can be omitted.

- **Polarity effect:** The polarity of the chamber potential (e.g. +200 V or -200 V) can have an impact on the dosimeter reading. The polarity correction factor k_{pol} is calculated via following expression:

$$k_{pol} = \frac{|M_+| + |M_-|}{2M} \tag{1.8}$$

  where M_+ and M_- are the respective electrometer readings and M is the reading with the

routinely used polarity.

- **Ion recombination:** Due to recombination of ions in an ionization chamber cavity ion recombination correction factors k_s have to be used. The calculation of k_s is complex and varies between continuous and pulsed beams. Further information can be found in [8].

With all correction factors absorbed dose to water is calculated via:

$$D_{w,Q} = M_Q N_{D,w,Q_0} k_{Q,Q_0} k_{TP} k_{elec} k_{pol} k_s \tag{1.9}$$

Two types of ionization chambers, a cylindrical Farmer chamber and a parallel-plate ionization chamber are described in section 3.5.

1.3.2 Other dosimeters used in particle therapy

Scintillation detectors: Scintillators are materials that emit light after they have been irradiated with ionizing radiation. They can be either organic (anthracene, stilbene) or anorganic (NaI(Tl), CaWO4). The scintillation light is than detected either by a photomultiplier (PM) or a charge coupled device (CCD). Some scintillation detectors show LET-quenching [7]. Scintillation detectors belong to active dosimetric systems. Following three other detector types are characterized as passive systems.

Alanine detectors: Alanine is an amino acid that produces unpaired electrons that are trapped by the surroundings and can be read out by electron spin resonance techniques. It is available in form of powder and pellets. Advantages of alanine include their linear dose behavior in therapeutic range and cumulative dose measurements throughout a treatment [7, 12, 13].

Film: Radiographic and radiochromic films are used in dosimetry due to their high spatial resolution, long term record and adjustable size. The easy handling and the unnecessity of a development process makes radiochromic film especially advantageous. A disadvantage of films is that they show LET dependent response [14].

OSL-dosimeters: In an optical stimulated luminescence detector (OSLD) electrons from ionizations are trapped at impurities in a crystal (mostly $Al_2O_3 : C$). After stimulation with

light of a certain wavelength these electrons can leave their traps and recombine with holes under emission of light. The light is detected by a PM-tube. This principle is equal to that of thermoluminescent detectors, only that for OSLDs a laser and not heat is used to stimulate the light emission [7, 10].

1.3.3 Thermoluminescent detectors

Thermoluminescence

Certain crystalline materials have the ability to store energy from ionizing radiation and release it later via emission of light. The emission of light can be triggered by different events. When heat is the actuator, the phenomenon is called thermoluminescence. Other types of luminescence include mechanoluminescence (light emission because of mechanical action on a solid), chemiluminescence (emission due to a chemical reaction), electroluminescence (emission because of electric current) or radioluminescence (emission due to ionizing radiation). It is important to remember that in case of thermoluminescence heat is only trigger for the emission of light and not the primary energy source. The origin of energy is the interaction of ionizing radiation with the crystal. Hence it would be more precise to call thermoluminescence heat stimulated luminescence [15].

The most materials that exhibit thermoluminescence are insulators with an ordered crystals structure with some natural or artificial impurities in it. This impurities cause defects in the structure and are essential for the phenomenon. Thermoluminescence is found in natural samples, used for dating applications, and in artificial produced crystals, used for dosimetry and can be described as a two step process: In the first stage shell electrons from crystal atoms are excited through ionizing radiation. In the second step heat is supplied and stimulates the emission of light (Fig. 1.4).

In the band structure of an insulator, the empty conduction band and the full valence band are separated by the band gap, a forbidden region for electrons. In thermoluminescent materials the Impurities in the crystal structure create energy levels within the forbidden region. These energy levels act as traps for electrons and holes. Ionizing radiation lifts electrons into the conduction band where some of them get trapped at defects in the crystal structure. Electrons remain in the metastable trapped state until external energy, in form of heat, is supplied. When electrons absorb a sufficient amount of thermal energy (activation energy) they are able to leave their traps and recombine with holes. The recombination results in the emission of visible light [15, 16].

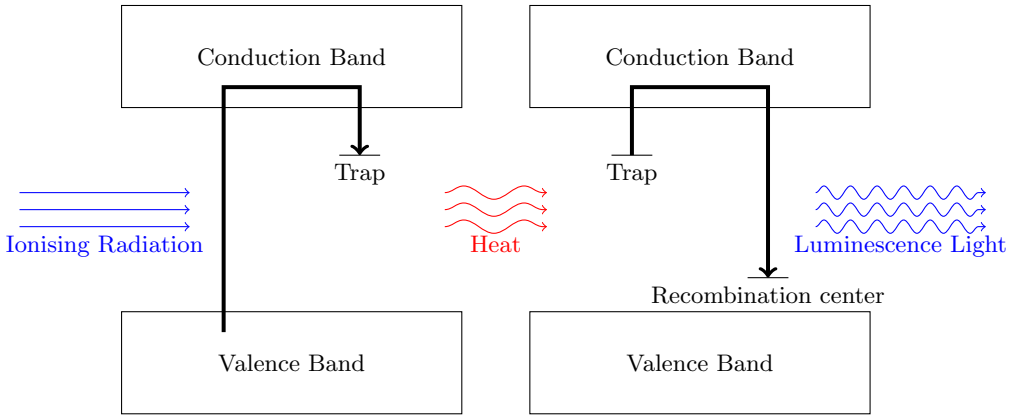

Fig. 1.4: Principle of TL; left: irradiation elevates electron to conduction band, electron gets trapped. right: heat releases electron from trap, light is emitted

Thermoluminescent materials typically have multiple trap levels with different activation energy (Fig. 1.5). As a consequence a sample that is heated with a temperature profile (e.g linear profile) will release electrons from shallow traps earlier than electrons from deep traps. This leads to the characteristic glow curve shape of thermoluminescent materials (see Fig. 1.6).

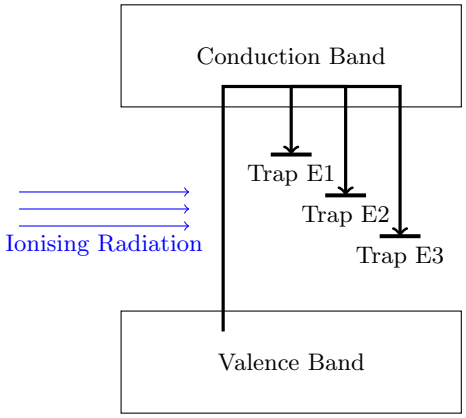

Fig. 1.5: Trap structure with multiple energy levels. This leads to glow curves with overlapping peaks as seen in Fig. 1.6.

A basic and simplified theoretical model for thermoluminescence was postulated in 1945 by Randall and Wilkins [17]. It describes the shape of a glow peak resulting from a single electron trap. This model excludes the possibility for an electron to be re-trapped immediately after leaving a trap and is therefor called "first-order kinetics". According to "first-order kinetics" the intensity of the light emitted by a thermoluminescent material as function of temperature is given as

$$I(T) = s \cdot n_0 \cdot exp\left(\frac{-E_t}{kT}\right) \cdot exp\left[-\frac{s}{\beta}\int_{T_0}^{T} exp\left(\frac{-E_t}{k\theta}\right) d\theta\right], \tag{1.10}$$

where s is the frequency factor, n_0 the number of trapped electrons, E_t the activation energy of a certain trap, k the Boltzmann constant, T the temperature, β the linear heating rate and T_0 the starting temperature. Randal and Wilkins approach is a simplified model and is not valid for all thermoluminescent materials. For TLD-100 the first order kinetic agrees well with experimental data [18]. For other thermoluminescent materials more sophisticated theoretical models were developed (e.g. second order kinetics and general order kinetics). When the glow curve is deconvoluted into individual peaks it's important that the correct theoretical model for individual peaks is used to get optimal results.

Thermoluminescence dosimetry

The fact that the emitted luminescence light is proportional to the absorbed dose, makes thermoluminescent materials useful for radiation dosimetry. For most dosimetric purposes artificially produced materials are used, this includes: lithium fluoride (LiF) doped with magnesium and titanium (LiF:Mg,Ti), LiF doped with magnesium, copper and phosphor (LiF:Mg,Cu,P), calcium fluoride with natural impurities (CaF2:nat) and calcium sulfate doped with manganese (CaSO4:Mn)(see also Tab. 2.1). Thermoluminescence dosimetry is a relative dosimetric method and besides the use in medical applications it's used for personal, environmental and space dosimetry. Below the most important characteristics of thermoluminescent detectors are briefly discussed.

Glow curve: The light output of a thermoluminescent material plotted as a function of the temperature during heat build up is called glow curve (see Fig. 1.6). Every peak in the glow curve corresponds to an energetic trap level between valence and conduction band. The closer a trap is to the conduction band the less energy is needed to release the trapped electrons, therefor shallow traps are associated with peaks at low temperatures and deep traps with peaks at high temperatures. The resulting glow curve is simply a superposition of peaks from different trap levels. A theoretical expression for a single glow peak was given in the section above (Eq. 2.6).[19]

Dose analysis: Since the emitted light is proportional to the absorbed dose the glow curve is used for dose determination in TL-dosimetry. The simplest approach would be to integrate the entire glow curve signal. Because electrons in traps with low activation energies are susceptible for release at room temperature, these low energy peaks are fast fading and make the readout and dose analysis process time dependent. For traps with higher activation energy thermal fading is

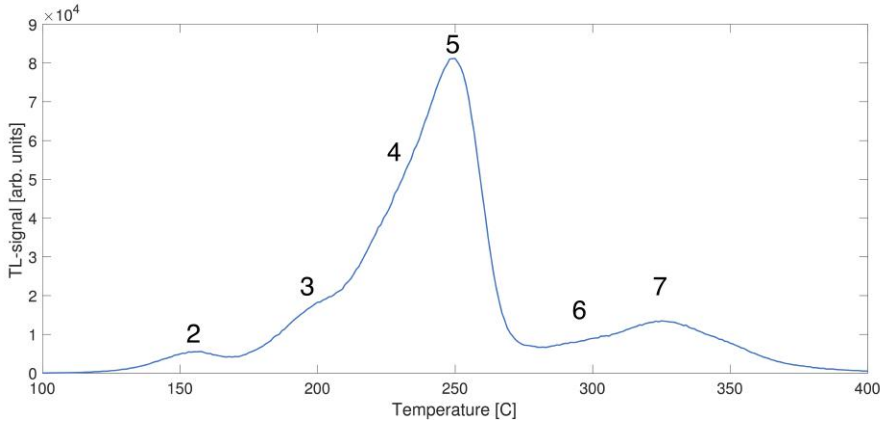

Fig. 1.6: Glow curve of TLD-100 with all visible peaks labeled.

negligible. Other approaches focus only on peak Nr.5 (highest peak in Fig. 1.6) for dose analysis. Either the maximum value (MAX) or a region of interest (ROI), around the main peak is used. The latter is more stable since not only a single value but an area under the glow curve is involved in the dose analysis. The most sophisticated and elaborated approach is to deconvolve the glow curve into individual peaks and integrate only the signal from the main dosimetric peak. This is connected to a high computational effort and is in most cases not needed for dose assessment. In section 4.4 a graphical representation of the various methods is presented. For all measurements within the scope of this thesis the ROI-method was used [20].

Dose linearity: For dosimetric usage a linear relationship between dose and thermoluminescence light is desired. In most common TLD materials this is not the case and nonlinear behavior can be observed. The response of LiF:Mg,Ti and many other materials is linear behavior only up to a certain dose level. After that supralinearity can be observed and at very high doses the light output saturates (Fig. 1.7). TLD-100 is usually linear up to a dose of 1 Gy and saturates at around 1000 Gy. The exact values depend on thermal treatment and readout procedure [19, 21, 22].

Radiation quality: The response of TLDs depends on the radiation quality. Therefore a corresponding calibrations in every radiation type in which TLDs are used has to be performed. Additionally thermoluminescent materials show energy dependence for some radiation types. For LiF:Mg,Ti irradiated with low energy photon radiation this energy dependence can influence the signal by up to 50% [19].

Thermal treatment: All thermoluminescent materials have to undergo a thermal procedure before they can be used for measurements. This thermal treatment, also called annealing, is

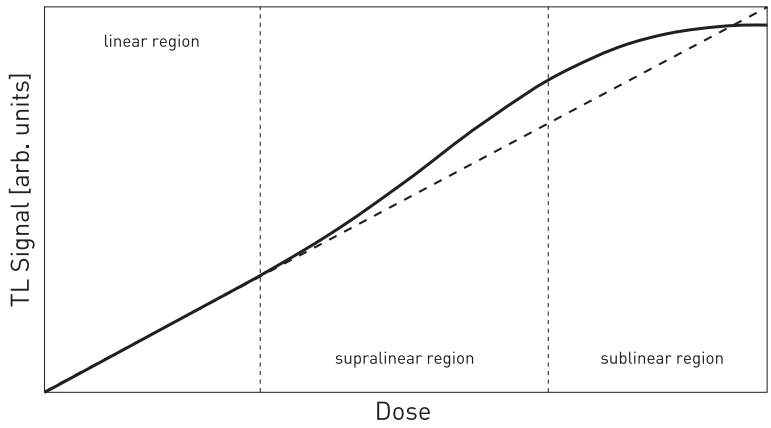

Fig. 1.7: Dose linearity of most common TL-materials.

needed to reset detectors and make them reusable. It removes all remaining trapped electrons and reestablishes the traps and luminescence centers in the crystal structure. Every thermoluminescent material has a specific thermal procedure. TLDs are very sensitive to changes in this treatment and hence it's utterly important that it's kept constant. The thermal treatment of LiF:Mg,Ti is described in detail in section 3.1.

1.4 MedAustron

MedAustron, center for ion therapy and research in Wiener Neustadt, is a dual particle facility for proton and carbon ion therapy, which started patient treatment at the end of 2016. The centerpiece of the facility is the synchrotron based MedAustron Particle Therapy Accelerator (MAPTA)(Fig. 1.8). The accelerator was designed according to PIMMS, the Proton-Ion Medical Machine Study [23], and is similar to the one at CNAO (Centro Nazionale di Adroterapia Oncologica) in Italy. Energies ranging from 62.4 MeV to 252.7 MeV are used clinically. For research purposes the accelerator can reach proton energies up to 800 MeV. The clinically utilized energies lead to a proton range in water (CSDA) reaching from 33 mm at 62.4 MeV to 386 mm at 252.7 MeV. So far only protons are available for clinical use. Commissioning of carbon ions will start in 2018. Carbon ions should be available for clinical use in 2019 and will be accelerated to energies between 120 MeV/u and 400 MeV/u which corresponds to ranges of 36 to 277 mm in water. MedAustron uses a quasi-discrete spot scanning technique, where steering magnets deflect a narrow particle beam and deliver dose to a large number of individual spots which form a target volume laterally. In depth the target is filled by particles of varying energy. Four irradiation rooms are available at MedAustron. The rooms have following beam configuration:

Fig. 1.8: 3D model of MedAustron with accelerator and irradiation rooms (source: [24])

- **IR1:** fixed horizontal beam
- **IR2:** fixed horizontal and fixed vertical beam
- **IR3:** fixed horizontal beam
- **IR4:** proton gantry (allows to move the nozzle around the patient and enables treatment from an arbitrary angle, planned to be operational in 2022).

IR2, 3 and 4 are used for patient treatment and clinical research. IR1 in contrast is solely dedicated for non-clinical research in the fields of radiobiology and (medical) radiation physics. All rooms are equally equipped with a robotic patient positioning system and a couch mounted imaging system [24] .

1.5 Motivation and Objectives

The main advantage of TLDs is their availability in many different shapes and sizes, their tissue equivalency and the lack of cables or electronics attached to them during irradiation. These properties allow a convenient use of TLDs in radiotherapy and radiation oncology, not only in various types of phantoms but also in in-vivo dosimetry, where TLDs are placed at the body surface or in body cavities. One of the main goals of in-vivo and surface dosimetry is to monitor the delivered dose during a treatment and to verify computations made in treatment planning. It can be especially valuable for dose measurements in radiation sensitive regions out of primary irradiation fields (e.g. eye lens, testicles, hip prostheses). In-vivo dosimetry enables inter-fractional adjustments of radiotherapy treatment and is a valuable tool to improve radiotherapy [25, 26].

In contrast to photon radiation, particle radiation has the advantage that most of the dose is released at a certain energy dependent depth, briefly before a particle stops. In-vivo dosimetry can be useful in particle therapy to measure skin-dose and dose at organs close to the distal end of particle beams. There the range uncertainties of particles can lead to deviations from the dose calculated in treatment planning systems [27].

But the use of thermoluminescent detectors in particle therapy is connected to challenges. TLDs show dependence on radiation quality, LET, dose level and the applied readout and resetting procedures [28]. Hence an in depth analysis of all these properties is necessary before TLDs can be used as reliable dosimeters for in-vivo and surface dose measurements in radiation therapy.

The aim of this work was to study the characteristics of TLD-100 detectors (ThermoFisher, USA) in combination with the available thermoluminescence oven and reader at MedAustron and to investigate the suitability of this system for in-vivo and surface dosimetry in particle beams. Therefore dosimeter specific correction factors, calibration in photon and proton beams and different dose analysis methods were studied. Additionally TLDs were irradiated and compared to radiochromic films in varying LET conditions that appear in clinically used spread-out Bragg peaks.

2 Equipment

This chapter is meant to give an overview about all used materials and instruments. The focus lies on thermoluminescent detectors and the used thermoluminescence reader.

2.1 Thermoluminescent detectors TLD-100

For all performed experiments, TLDs of type TLD-100 supplied by Thermo Fisher Scientific, USA were used. TLD-100 is a Lithium-Fluoride crystal doped with Magnesium and Titanium (LiF:Mg,Ti). It is one of the most commonly used thermoluminescent detector materials. In contrast to TLD-600 and TLD 700, it consists of a crystal with a Li^6/ Li^7 ratio equal to that in natural occurrences, while TLD-600 and TLD-700, also LiF crystals, are enriched with Li^6 or Li^7. TLD-100 is available in many different physical shapes and sizes including powder, rods, cubes and disks. For the following experiments TLD-100 in shape of disks was used with a diameter of 4.5 mm and a thickness of 0.9 mm (Fig. 2.1a).

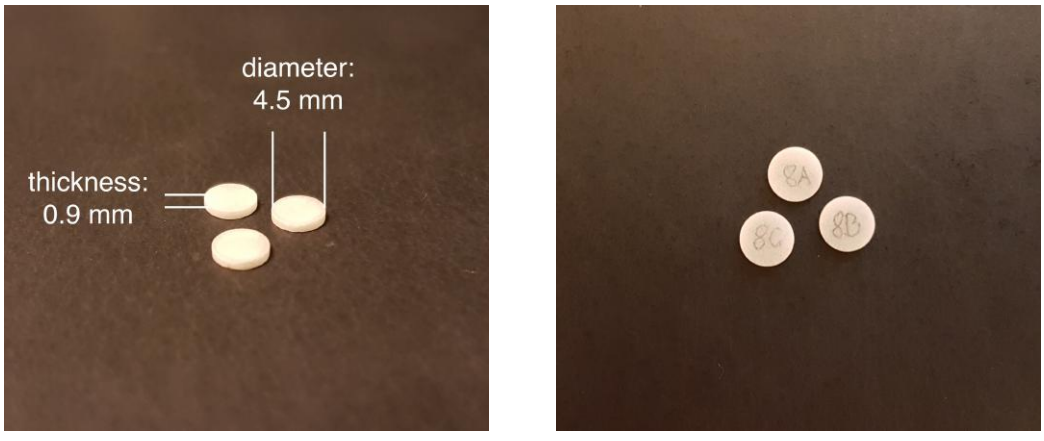

(a) **(b)**

Fig. 2.1: a) Shape and dimensions of the used TLD 100 dosimeters b) Labeling on TLDs

Advantages of the disk shape and the dimensions include easy handling, the ability to conveniently use them in phantoms and their good spatial resolution. Currently there are 192, type TLD-100 detectors available at MedAustron. They are separated into eight sets of 24 TLDs each. To distinguish individual TLDs and to keep track of them during experiments they are labeled with an alphanumerical code. Every TLD is marked with a number to define the set and a character

from A to X to define the position inside the set (Figure 2.1b). A soft mechanical pencil was used to label TLDs. The labelling influences the light output of TLDs and should therefore be done prior to all calibration and correction measurements. All experiments of this work were conducted with labeled TLDs. During all readout and annealing procedures the label on the TLDs was stable and did not vanish. For all performed measurements TLDs were placed with the unlabeled side facing the beam, to prevent any influence on the results. In appendix D recommendations for quality assurance of the detectors are presented.

Specifications and characteristics of TLD-100 and other common TL-materials are listed in Tab. 2.1 [19].

Tab. 2.1: Specifications of common TLD-materials in comparison to LiF:Mg,Ti [19]

TL material	**LiF:Mg,Ti (TLD-100)**	**LiF:Mg,Cu,P**	**$Li_2B_4O_7$:Mn**	**CaF_2:nat**	**$CaSO_4$:Mn**
physical density (g/cm^3)	2.64	2.64	2.3	3.18	2.61
effectiv atomic nr.	8.2	8.2	7.4	16.3	15.3
sensitivity for Co_{60} (relative to LiF:Mg,Ti)	1	about 30	0.3	23	70
main peak temp. (°C)	195	210	200	260	110
maximum wavelength of emitted light	400	380	600	380	500
fading of main peak	< 10% per year	2% in 3 months	10% per month	< 10% per year	50% per day

Annealing

As every thermoluminescent material, TLD-100 needs to be thermally treated in order to be prepared for a measurement. The annealing procedure for TLDs based on LiF:Mg,Ti is somewhat more complex than for other materials because it consists of two steps. A high temperature annealing at 400°C for one hour is followed by a low temperature procedure at 100°C for two hours. The high temperature level removes all remaining trapped electrons that have not been liberated during readout. While the low temperature level reestablishes the trap structure in the crystal. This procedure is performed in a special TL-oven and has to be as equal as possible for consecutive annealing cycles to get repeatable results [29]. Figure 2.2 shows a time-temperature profile of the annealing procedure.

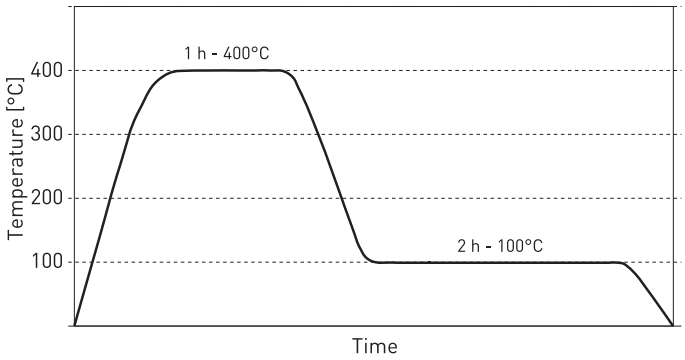

Fig. 2.2: Time-temperature profile of annealing procedure for TLD 100

Additionally, the detectors can be heated up to 100°C for 10 minutes before being read in the TLD-reader. This leads to the removal of the first unstable and fast fading peaks. This procedure is optional but should be performed if the entire glow curve is integrated for dose determination. Otherwise, due the the fast fading peaks, the time between irradiation and readout influences the measured dose. In the following measurements with TLDs, this additional procedure was not carried out, only a region of interest (ROI) around the main peak, where fading is very low, was used for dose determination (Figure 3.1).

2.2 Risø TLD reader

As described in section 2, the electrons in the detector material, will be able to leave their trapped state when the detector material is heated up. A fraction of these electrons will recombine with holes and emit light. Hence a TL-reader, which performs the heating and measures the intensity of the emitted light, is needed for TL-dosimetry. [19].

Different approaches for heating systems exist, the most simple technique uses an ohmic heating plate in combination with a temperature sensor (e.g. thermocouple) to control and monitor the heating. More sophisticated approaches include a stream of a hot gas or lasers to heat the detector. TL-dosimeters are very sensitive to a change in the heating conditions, so all of these methods have to be highly reproducible to keep the error resulting from the heating system as small as possible.

The emitted light is almost always detected by a photomultiplier tube (PMT). A PMT is a highly sensitive detector that consists of a photocathode, multiple dynodes and an anode. The photocathode converts the incoming photons into electrons. The dynodes are connected to a

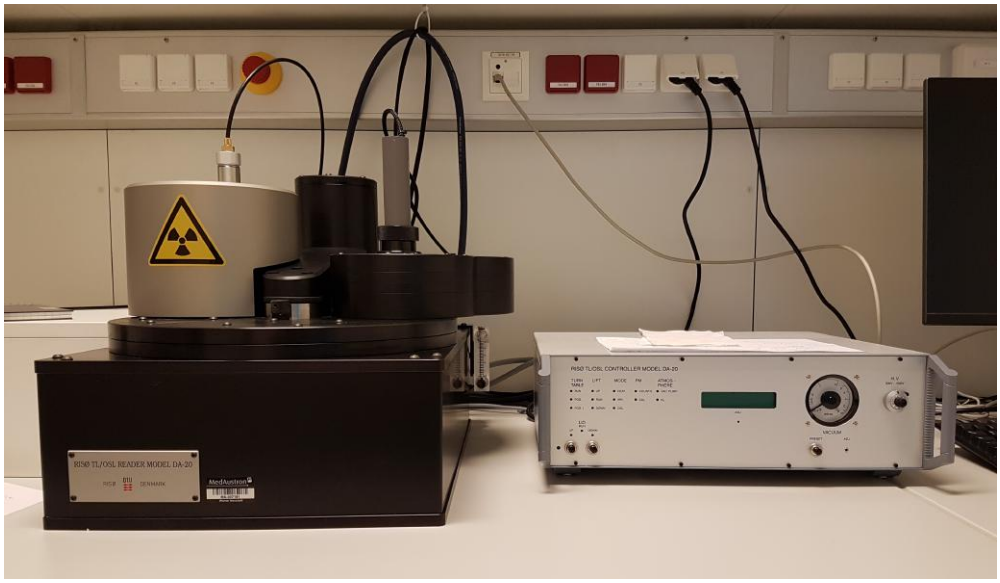

Fig. 2.3: Risø TLD reader with readout device on the left and the controller unit on the right. The beta irradiator is marked with a yellow sticker

high voltage supply and accelerate the electrons. At every dynode the accelerated electrons liberate secondary electrons which leads to an amplification of the signal and after several steps this signal can be measured at an anode and further processed in readout electronics.

At MedAustron a Risø DA20 TL/OSL reader from DTU Nutech, Denmark is in use. The reader is not only suitable for thermoluminescence measurements but can also be used for optical stimulated luminescence (OSL) measurements. The Risø reader consist of two parts, a controll unit and the readout device itself (see Figure 2.4). The controll unit is connected to a PC and is responsible for the proper execution of programs and sending data from the reader back to the PC. The readout device is equipped with a sample wheel, heating element, photomultiplier tube, filter wheel and a built-in beta source [30]. In the following section the individual parts will be briefly described.

Heating element:

The heating element of the Risø DA20 TL/OSL reader is made out of Kanthal, a Fe-Cr-Al alloy, and mounted on a height adjustable platform. This platform rises a sample holder, in form of a small cup or disk, up and brings it into the measurement position directly in front of the photomultiplier tube. The temperature of the heating element is monitored by a chromel-alumel (type-k) thermocouple and is part of a feedback loop to control the temperature. With heating rates from 0.1°C to 10°C a maximum temperature of 700°C can be reached. The measurement

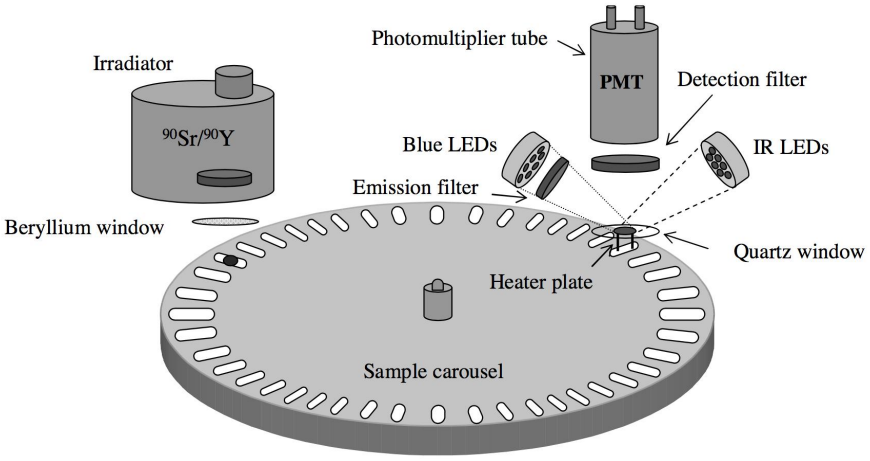

Fig. 2.4: Schematic drawing of the Risø DA20 TL/OSL reader with sample wheel, PMT, heater plate, irradiator and some additional elements used in OSL (image source: [31])

chamber is flooded with a constant flow of nitrogen to cool the heating element and to reduce spurious light emission.

Photomultiplier Tube:

The Risø TLD-reader is equipped with a bialkali EMI 9235QA photomultiplier tube which sits on top of the lid. It has extended UV response and maximum detection efficiency between 300 and 400nm. During readout the distance between sample and PMT is 55mm.

Sample wheels:

The reader comes with two different sample wheels where detectors are placed on for the readout. One is equipped with disks, the other one with small cups. Each wheel has 48 positions. On the sample wheels, disks and cups are not permanently mounted (see Figure 2.5). They will be lifted up by the heating element to bring them directly in front of the photomultiplier tube. Cups and disks can be removed for maintenance and cleaning purposes. Because there is a noticeable difference in signal between the two (for details see [32]), either cups or disks have to be used throughout all experiments to get consistent results. During this work cups were used for all measurements.

Fig. 2.5: Sample holder in form of disk and cup (left) and sample wheel for cups (right)

Beta irradiator:

On top of the reader a $^{90}Sr/^{90}Y$ beta irradiator is mounted (see Figure 2.4). This source emits beta particles with a maximum energy of 2.27 MeV and has a half life of 28.8 Years. In April 2017 the dose rate in TLDs was measured to be approximately 0.3 mGy/s [33]. The built-in source was used for irradiation of TLDs to determine individual sensitivity factors (more details in section 4.1).

Filters:

The reader features two filter wheels with 4 positions. The use of filters is controlled via the sequence editor software. They are located in front of the PMT and due to the mounting of the filter wheels (on top of each other), two filters can be used at the same time. The reader at MedAustron is equipped with a U340 5mm, a U340 2.5 mm, two neutral density filters and a blue filter. Most of these filters are used in OSL for separating stimulation and emission light, but they can also be used during TL-measurements to reduce the light intensity. At higher light intensities the PMT will saturate, hence the filter set allows the measurement of higher intensities and doses. For this work the U340 5mm filter was used for all measurements.

Software:

The reader comes with the following software:

- Sequence editor

- Analyst
- Control program

The sequence editor is a spreadsheet-like program where all relevant parameters for readout and irradiation with the built-in source can be set. The Analyst software is used to view, edit and analyze data that is produced by the Risø reader. It also allows the conversion of the reader specific file format to simple text files, which is needed for further analysis in different software. The control program is used for maintenance and troubleshooting purposes and allows the change and test of all functions/settings of the reader.

Sequence:

The reader is very versatile and it is possible to customize all parameters for the readout in the sequence editor. This includes settings like maximum temperature, heating rate, pre-heat temperature/time, filters, number of data-points that are recorded, use of nitrogen and many more. The readout sequence is different for every TL-material. At MedAustron following sequence settings are established for TLD-100:

- Pre-heat: none
- Final temperature: 400°C
- Heating rate: 5°C/s
- Number of datapoints: 400
- Nitrogen: always on
- Upper filter: U340 5mm
- Lower filter: none

Some recommendations for maintenance and quality assurance of the Risø TLD-reader are discussed in appendix D.

2.3 TLD annealing oven

TLDs were annealed at Vienna General Hospital (AKH) in a TLDO TLD-oven from PTW Freiburg, Germany. This oven was designed solely for the annealing of TLDs, and especially for

LiF:Mg,Ti. A heating element produces a hot air stream that is circulated by a built-in fan. This leads to a homogenous temperature distribution over the whole oven chamber. The oven has the ability to heat up to 400°C in a very short time and keeps the temperature with an accuracy of 1°C [34].

For annealing the detectors were put on a metal tray with cutouts for TLDs and covered with a metal lid. Two optimized programs for LiF:Mg,Ti are programmed into this oven. One for pre-irradiation annealing (see Figure 2.2), at 400°C for one hour followed by 100°C for two hours, and one to preheat TLDs before readout, at 100°C for 10 minutes. The pre-irradiation annealing program needs about 4h and 30min, including the cooling in between the temperature levels. Figure 2.6 shows the oven with an opened door and detectors inside.

Fig. 2.6: TLD annealing oven at AKH

TLD oven at MedAustron

At MedAustron a LT3/11 oven from Nabertherm, Germany is available for annealing of TLDs. This oven is not dedicated for TLD annealing and showed insufficient annealing performance and couldn't be used for preparation of TLDs. Therefore it was necessary to use the oven at AKH Wien / MedUni Wien. Problems that occurred with the oven include inaccurate temperature readings by a built-in thermocouple and inhomogeneous heat distribution inside the oven because of the lack of a fan. To improve the performance, an insert, made out of metal, was built in-house

and tested extensively. Recent results with the improved oven showed that the oven might be suitable for future use at MedAustron [32].

2.4 EBT3 and EBT-XD films

EBT3 and EBT-XD films from GAFchromic (USA) are self developing radiochromic films that are used in radiation dosimetry due to their high spatial resolution, possibility of multiple readouts, storage of the result and the customizability of their size [7]. EBT3 films are optimized for doses between 0.2 and 10 Gy and are therefore qualified for application in radiation therapy. The films consist of an 28 μm thick active layer, with an active component, a marker dye and stabilizers between two 125 μm thick matte-polyester substrates.

EBT-XD films are optimized for doses higher than 10 Gy and can be used in a region from 0.4 to 40 Gy. They feature an active layer with a thickness of 25 μm also comprised by two matte-polyester substrates of 125 μm thickness.

Both types can be handled in ambient light but should be stored protected from radiation sources at a dark place. For evaluation of the irradiated films a EPSON Expression 11000XL flatbed scanner was used [35]. The red channel from the scanned image was extracted and the optical density (OD) was calculated with following expression

$$OD_{red} = log(\frac{2^{16}}{PV_{red} + 1}) \tag{2.1}$$

A calibration for the optical density of EBT3 and EBT-XD films in protons was available at MedAustron [36]. EBT3 and EBT-XD films were used to compare their response to TLDs in a spread-out Bragg peak.

2.5 Ionization chambers and electrometer

Ionization chambers are gas filled detectors that detect ionizing radiation by collecting the produced charge carriers. They consist of an anode and a cathode with a high voltage supply and create an electric field in the sensitive gas volume. When ionizing radiation enters the sensitive

volume ion pairs are created. The electric field accelerates the ions to anode and cathode and as a result a charge or current can be measured. This is proportional to the absorbed dose in the sensitive volume. Figure 2.7 shows the basic setup of an ionization chamber with a parallel anode-cathode setup. [10]

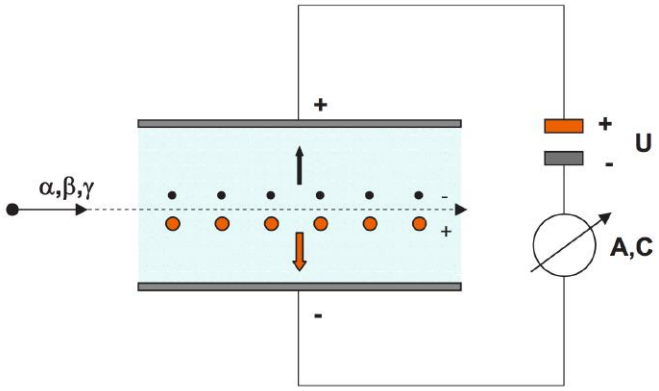

Fig. 2.7: Basic setup of ionization chamber with parallel anode-cathode configuration (image source: [10])

Ionization chambers are sensitive to the surrounding environmental condition, therefore their reading has to be corrected by temperature and pressure by following formula

$$k_{T,P} = \frac{(273.2 + T) * P_0}{(273.2 + T_0) * P} \tag{2.2}$$

where T is the temperature in the sensitive volume in °C, T_0 the calibration temperature (20°C), P the atmospheric pressure at the measuring site in hPa and P_0 the atmospheric pressure for calibration (1013.25 hPa).

Farmer ionization chamber

The Farmer ionization chamber, type 30013 from PTW Freiburg, Germany is a thimble waterproof ionization chamber used for absolute dosimetry [37]. It has a sensitive volume of 0.6 cm^3. The chamber should be supplied by a voltage of 400 V and connected to a compatible PTW electrometer. Farmer chamber, shown in Fig. 2.8 a, was used for calibration measurements in the Co60 source at AKH Wien/MedUni Wien.

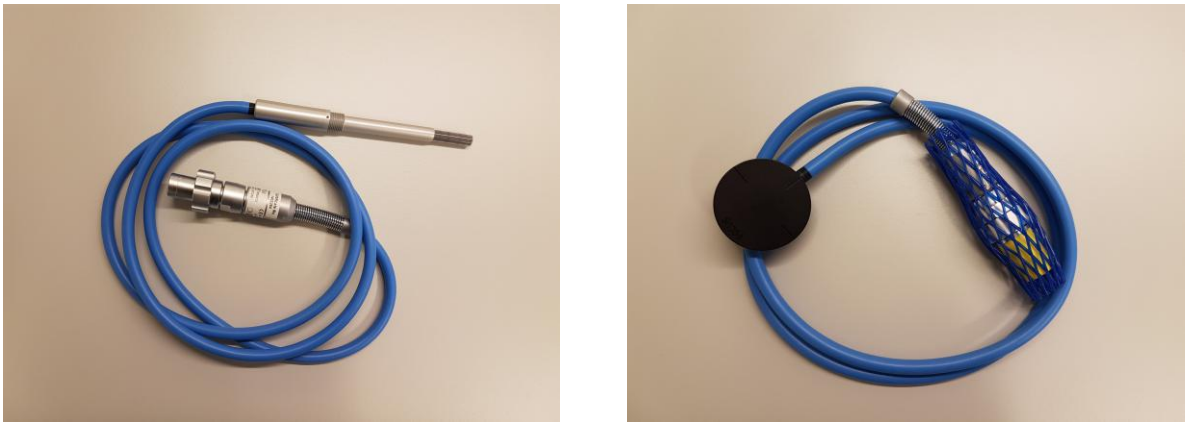

(a) (b)

Fig. 2.8: Farmer ionization chamber (left) and Roos ionization chamber (right)

Roos ionization chamber

The Roos ionization chamber, type 34001 is a waterproof plane parallel ionization chamber from PTW Freiburg, Germany. A sensitive volume of 0.35cm^3 behind the entrance window of 1.13 mm (PMMA and graphite coating) is used to detect ionizing radiation [38]. The difference between Roos and Farmer chamber is the shape of anode and cathode. If very high spatial resolution in direction of the beam is needed, the thin sensitive volume of the Roos chamber, with the parallel anode-cathode setup, is an advantage. Roos chamber was used for all measurements in the proton beam.

Unidos electrometer

In order to measure the charge that has been collected in the chamber and supply it with the needed voltage, ionization chambers have to be connected to electrometers. For measurements at MedAustron a Unidos webline from PTW Freiburg, Germany was used while for measurements with the ^{60}Co source at AKH Wien / MedUni Wien a Unidos E, also from PTW Freiburg, was used. The Unidos webline is a versatile electrometer with a colored display and the ability to be controlled over network while Unidos E has the same basic functions as Unidos webline but lacks the colored display and network functionality. [39].

2.6 RW3 slab phantom

The RW3 slab phantom (PTW Freiburg, Germany) consists of various slabs with a size of 30 x 30 x 30 cm^3. Slabs have thicknesses of 10 mm (29 pieces), 5 mm (1), 2 mm (2) or 1 mm (1) [40]. All slabs together form 300 mm in depth, hence measurement positions from 1 to 300 mm in steps of 1 mm can be created by aligning slabs of different thickness. Phantom material is RW3 (Goettingen white water) which is approximately water equivalent over a wide range of energies with a water equivalent thickness of 1.041. The phantom is designed to be used in combination with ionization chambers and extra plates with inserts for Roos and Farmer ionization chamber are also available at MedAustron. In order to keep the slabs in place, a proper RW3 slab holder (PTW Freiburg, Germany) was used.

Customized TLD slab phantom

As a part of this work a TLD slab phantom was designed and produced in-house. It consists of seven 1 mm RW3 plates were customised in-house. The slabs have 5, 6 or 7 holes with a diameter of 4.6 mm. Figure 3.8 shows plate number 1 in close up and the entire plate number 7.

(a) **(b)**

Fig. 2.9: Customized RW3 slabs. a) Close up of plate number 1 b) Complete plate number 7.

All seven slabs can be used with TLDs at the same time without mutual shielding. TLDs are distributed over a circle with a radius of about 6 cm. Figure 2.10a gives an overview of the distribution of all holes and Figure 2.10b shows a planar x-ray image of the whole phantom,

where all plates are put together. Plate number 1 was designed to be used as a calibration plate. Five central TLD positions are distributed over roughly the same area as the Roos chambers surface. In total 41 TLDs can be placed in 7 different depths if the plates are fully equipped with detectors. This phantom in combination with the RW3 slab phantom allows measurements along the Bragg curve or spread-out Bragg peaks in several depths at the same time and reduces the measurement time significantly. In Appendix A the individual RW3 plates and the dimensions of the drillings are shown.

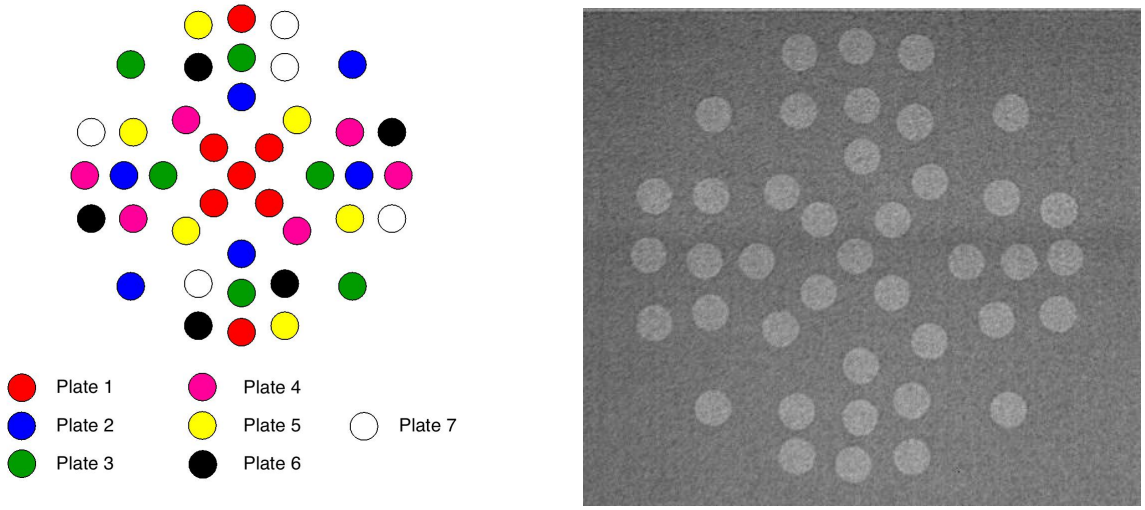

(a) **(b)**

Fig. 2.10: a) Color coded overview of the in-house modified RW3 plates. b) Xray image of assembled RW3 phantom.

2.7 ^{60}Co source

^{60}Co, with a half life of 5.27 years, can be produced inside reactors by irradiating stable ^{59}Co with neutrons. It decays via a beta decay to the stable isotope ^{60}Ni. ^{60}Ni is activated and emits gamma rays with energies of 1.17 and 1.33 MeV. Figure 2.11 shows the decay scheme. An advantage of ^{60}Co is the high intensity gamma radiation in combination with the long half life. This makes it suitable for use in radiotherapy but also as calibration source.

A Theratron 780C radiotherapy unit was used for ^{60}Co irradiations. This machine, located at AKH Wien / MedUni Wien, is utilized as a calibration source for all kinds of detectors. The field size and irradiation time can be set to fit the experimental needs. The field size is adjusted directly on the device while the irradiation time is set at a control unit in an adjacent room.

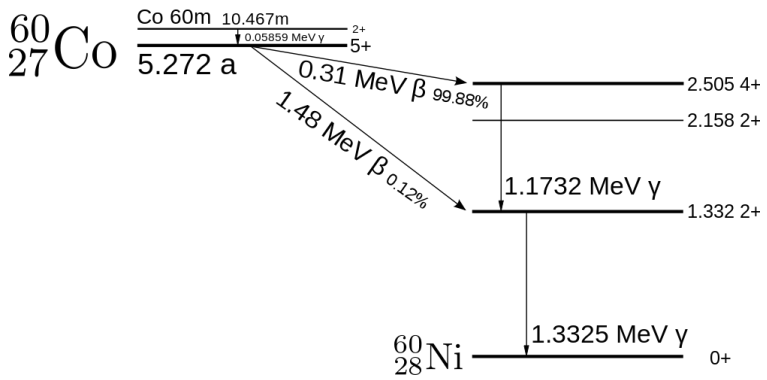

Fig. 2.11: Decay scheme of ^{60}Co

In August 2017 5 minutes of irradiation lead to a dose of about 1 Gy (measured with Farmer chamber and the PMMA chamber holder, described in section 4.2).

2.8 MATLAB

MATLAB (Mathworks, USA) is a software environment for matrix manipulations, plotting, implementation of algorithms, creation of user interfaces and interfacing with programs written in other languages. MATLAB was used for all measurements to analyze and display the data. Scripts were written for reading output files from the TLD reader, determine maximum value of glow curves, integrate glow curves over a specified region of interest. All used scripts are attached and described in Appendix B.

3 Measurements

3.1 Comparison of glow curve analysis methods

As mentioned in 2.3.2 there are multiple possibilities to analyse the glow curve and obtain a TLD signal from it. To study the effect of different glow curve analysis methods on the measurement results, TLD data from the ^{60}Co calibration was used and analyzed with three different methods. The 'MAX'-method uses the global maximum of the glow curve for dose determination while the 'ROI'-method uses a confined region around the main-peak. In addition to these two a glow curve deconvolution into individual peaks was performed. For this task the software tool GLOWFIT [41] was used. MAX and ROI method were computed using MATLAB scripts which were written in the frame of this work (Appendix B). Figures 3.1 and 3.2 give graphical representation of the different methods.

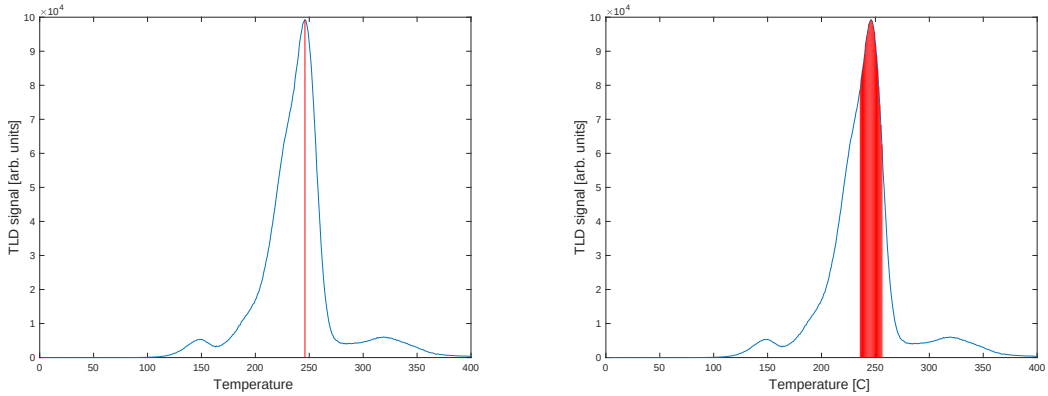

Fig. 3.1: Graphical representation of MAX (left) and ROI (right) method for dose determination. The red line/area indicates which data was used for dose determination.

3.2 Individual sensitivity factors for TLD 100

When a set of TLDs is irradiated with a uniform dose, every individual TLD responds slightly different. This is due to variations in the physical properties of each detector like size, crystal structure and usage. The sample-to-sample uniformity of TLD 100 from Thermo Fisher Scientific was stated by the manufacturer to be within ±15%. To check this uniformity as well as the reproducibility of the used TLDs, 48 of the 192 TLDs were selected and irradiated for 300 seconds

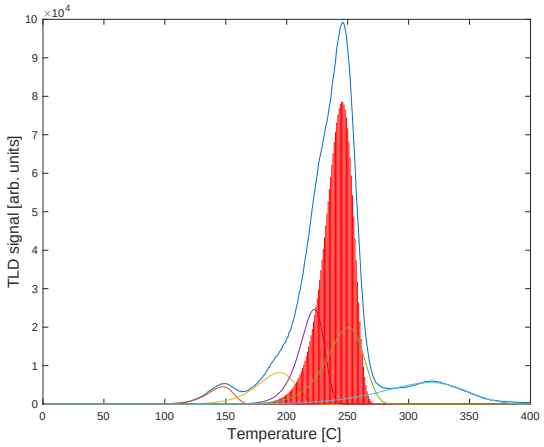

Fig. 3.2: Graphical representation of the deconvolution method. The red area indicates which data was used for dose determination.

with the built-in beta source inside the reader. This corresponds to a dose of about 0.1 Gy. The exact delivered dose is not of interest as long as all 48 TLDs are irradiated with a uniform dose. TLDs were read with the Risø TLD reader immediately after the irradiation. A readout sequence with the standard parameters, described in section 3.2, was used. The whole procedure, including irradiation and readout, was repeated three times to obtain statistical parameters. Individual sensitivity factors provide information about uniformity and reproducibility of TLDs. Moreover they can also be used to correct the response of every single TLD and decrease the variation in measurements. Below the procedure of determining the individual sensitivity factors is described.

Procedure for determination of individual sensitivity factors S_i [29]:

1. Annealing of TLDs
2. Irradiation of TLDs inside the reader for 300 seconds with built-in beta source
3. Readout of TLDs
4. Calculation of mean response of all 48 TLDs

$$\overline{M_1} = \frac{1}{48} \sum_{i=1}^{48} M_i \,, \tag{3.1}$$

   where M_i is response of individual TLDs

5. Calculation of $\overline{M_2}$ and $\overline{M_3}$ by repeating steps 1 to 4

6. Calculation of the average mean value of the 48 TLDs for every irradiation/readout by

$$\overline{\overline{M}} = \frac{1}{3}\sum_{j=1}^{3}\overline{M_j}\,, \tag{3.2}$$

   with j as irradiation number

7. Calculation of average response of every single TLD

$$\overline{M_i} = \frac{1}{3}\sum_{j=1}^{3}M_{i,j}\,, \tag{3.3}$$

   where i is the TLD number and j the irradiation number.

8. The individual sensitivity factors S_i are then defined as

$$S_i = \frac{\overline{\overline{M}}}{\overline{M_i}} \tag{3.4}$$

Hereby obtained individual sensitivity factors S_i are multiplying factors. Measurement results can be corrected by multiplying the signal from a TLD by the according sensitivity factor S_i:

$$M_{i,corrected} = M_{i,raw}\cdot S_i\,. \tag{3.5}$$

To quantify the variation in a measurement with multiple TLDs the relative standard deviation (RSD) or coefficient of variation (CV) is used. It is defined as ratio of standard deviation to the mean:

$$CV = \frac{\sigma}{\mu}\,, \tag{3.6}$$

where σ is the standard deviation of TLDs in a measurement and μ the mean value of these TLDs.

3.3 Calibration in ^{60}Co

TLDs are used for relative dosimetry, their thermoluminescent light output is typically related to a calibrated dosimeter to use it to measure the absorbed dose. Farmer ionization chamber,

connected to a Unidos E electrometer, was used as a calibrated dosimeter for TLD measurements in the ^{60}Co beam at AKH Wien / MedUni Wien. TLDs and the Farmer chamber were irradiated at equal positions using a PMMA block, mounted 30 cm away from the ^{60}Co source. The PMMA block is adapted to accommodate the farmer chamber. For TLDs a custom PMMA TLD holder in the shape of a Farmer chamber was available at AKH. Three TLDs can be inserted into the holder at a time. The PMMA TLD-holder is shown in Fig. 3.4. The field size of the ^{60}Co unit was set to 10 x 10 cm^2.

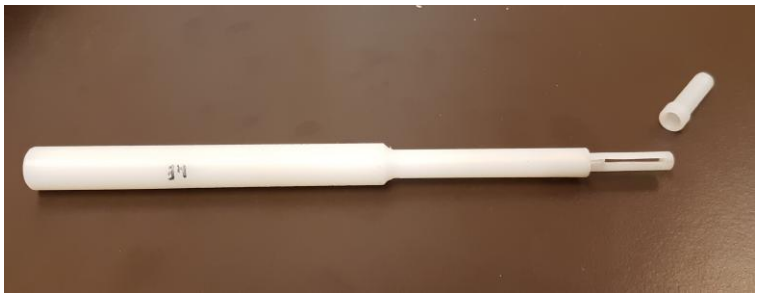

Fig. 3.3: TLD holder in shape of the farmer chamber. At the tip of the holder three TLDs can be placed next to each other in the small slit

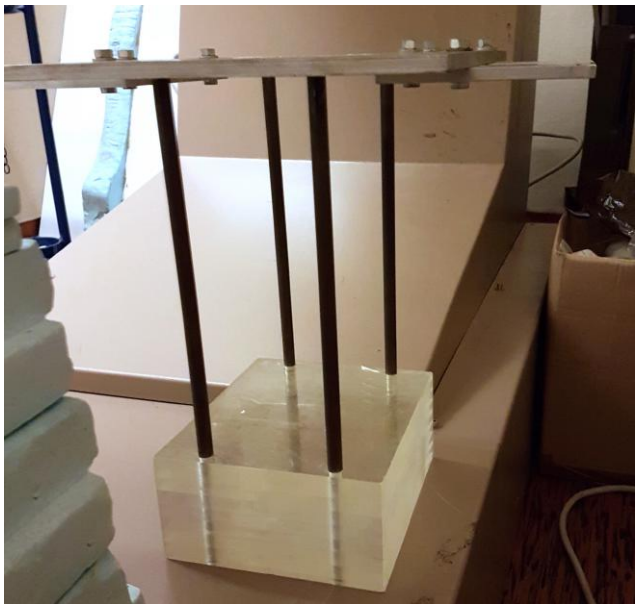

Fig. 3.4: PMMA block for irradiation of farmer chamber and TLDs. The block was mounted at 30 cm distance from the ^{60}Co source.

Irradiation times between 60 and 1500 seconds were used to get a corresponding dose range of 0.2 to 5 Gy. The used irradiation time and the corresponding dose levels are listed in table 3.1. For dose levels up to 2.2 Gy, two sets of three TLDs were irradiated. Because of the long irradiation times for higher doses (3 and 5 Gy), only one irradiation with three TLDs was carried out. Due to the long irradiation times, measurements with the ionization chamber were only conducted multiple times for lower doses (0.2, 0.5 and 1 Gy) and extrapolated for higher ones.

Tab. 3.1: Irradiation time and corresponding dose levels measured with Farmer ionization chamber

Irradiation time [s]	**60**	**150**	**300**	**450**	**550**	**600**	**660**	**900**	**1500**
measured dose [Gy]	0.20	0.50	1.00	-	-	-	-	-	-
extrapolated dose [Gy]	-	-	-	1.50	1.83	1.99	2.19	2.99	4.98

To quantify the linearity of the TLD response, the linearity index was used [42]. It is defined as:

$$f(D) = \frac{\frac{M(D)}{D}}{\frac{M(D_l)}{D_l}}\,, \tag{3.7}$$

where $M(D)$ is the TLD response at a certain dose D and $M(D_l)$ is the TLD response in a dose region D_l where linear behavior is known or assumed.

3.4 Calibration in proton beams

Main use of TLDs at MedAustron is foreseen to be in proton beams. The response of TLDs varies with the radiation type and therefor another calibration, in addition to ^{60}Co, was conducted in proton beams.

Single energy irradiation plans at 179 MeV with a fieldsize of 10 x 10 cm^2 and doses from 0.2 to 2.2 Gy were created to generate a calibration curve for TLDs. The detectors were positioned in a PMMA plate with cutouts for TLDs (see Fig.3.5) in the center of the field. They were distributed over 2 x 2 cm^2 to cover the area of the calibrated Roos ionization chamber. Every irradiation plan was first measured twice with the Roos chamber connected to Unidos webline electrometer. The ionization chamber was positioned at a depth of 19 mm in RW3, which corresponds to 20 mm water equivalent depth. TLDs were positioned at the same depth as the Roos chamber and for every dose level five TLDs were irradiated.

3.5 Spread-out Bragg peak irradiation with passive detectors

As stated in [7, 20, 43, 44, 45], TLDs show a linear energy transfer (LET) dependent response in high LET regions, which appear at the end of Bragg curves and spread-out Bragg peaks (see figure 3.6). This phenomenon, also seen in other passive detectors (film, alanine), is also known as quenching. When TLD-100 is used in modulated proton beams this effect seems to be reduced

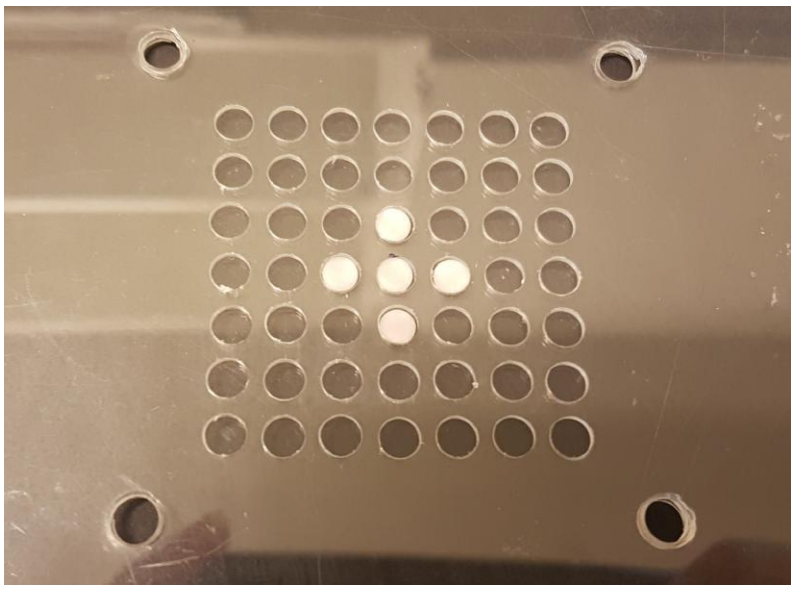

Fig. 3.5: TLDs in PMMA holder used for calibration in proton beams

[7]. Preparatory measurements to investigate and establish a quenching correction for LiF-TLDs were made in a spread-out Bragg peak. For comparison EBT3 and EBT-XD films were irradiated under same conditions.

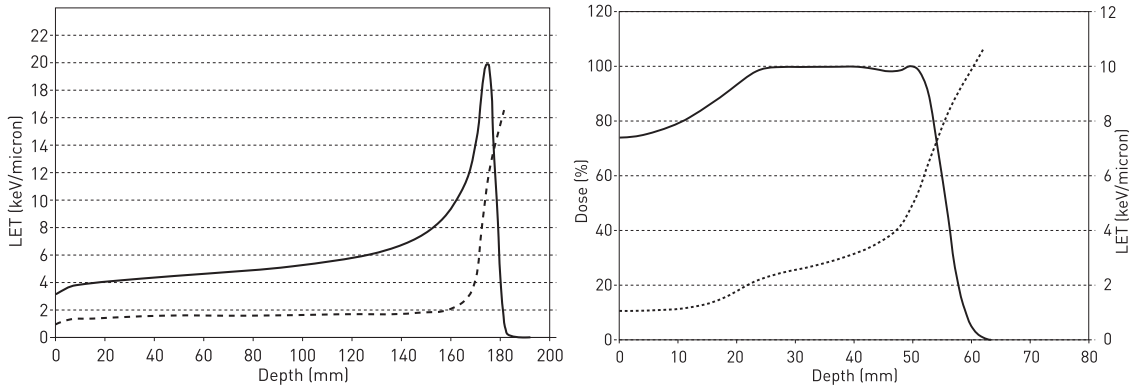

Fig. 3.6: Change of dose averaged LET (dashed line) with increasing depth and depth-dose profile (solid line) for pristine Bragg peak (left) and SOBP (right). Data from [7].

Plan design and TLD irradiation

A cylindrically shaped target was designed on the RW3 phantom in the treatment planning system (TPS - Raystation, Raysearch, Sweden). The target with 120 mm in diameter started at depth of 33 mm. The plan was calculated with the pencil beam algorithm and for the modulation depth of 8 cm, proton energies between 69.5 and 133.8 MeV were used. A combination of RW3 slab phantom and the in-house developed TLD phantom, described in detail in section 3.6, was used to position TLDs along the beam. TLDs were placed at water equivalent depths of 20.8,

42.7, 75.0, 86.4, 94.7, 106.2 and 110.3 mm in the RW3 slab phantom. 41 TLDs were irradiated in this configuration at the same time in seven different depths along the beam, without shielding each other. The plan was irradiated in 12 minutes and the measurement with two sets of 41 TLDs was repeated twice.

Tab. 3.2: Positions of TLDs and EBT3 Films (WED in mm)

Position	IC	TLDs	FILM1	FILM2
1	20.9	20.8	20.8	20.8
2	42.8	42.7	42.3	42.3
3	-	-	63.9	63.9
4	75.1	75.0	75.0	75.0
5	86.5	86.4	86.1	86.1
6	94.9	94.7	95.1	95.1
7	-	-	102.1	-
8	106.3	106.2	106.9	-
9	110.5	110.4	110.7	-
10	-	-	112.5	-

Film irradiation

Radiographic films of type EBT3 and EBT-XD were positioned in the RW3 slab phantom at the same water equivalent depths as TLDs, or as close as possible to TLD positions. The same plan designed for TLD irradiation was applied for films. Similar to the TLD measurement, two sets of films were irradiated. In the fist set ten depths were measured (7 of them equal to TLDs), while in set 2 only six depths equivalent to TLDs were measured. Additional film in parallel orientation was placed at the end of SOBP and the distal fall off in the second measurement set. This was part of a different experiment and will not be discussed in this work. EBT3 and EBT-XD films were cut in 4 x 4 cm^2 pieces and positioned in between two slabs of RW3 in the center of the target volume. At every measurement position EBT3 and EBT-XD films were put aligned in alternating order. Table 3.2 lists the water equivalent depth of the measurement positions of TLDs, films and the ionization chamber in the RW3 slab phantom.

4 Results and Discussion

4.1 Comparison of glow curve analysis methods

For comparison of the different glow curve analysis methods, data from the ^{60}Co calibration was used. Every glow curve was analyzed with the three described methods and the results were normalized to 1 Gy obtained with the respective method. The data was not corrected with individual sensitivity factors for this comparison. The results are given in Tab. 4.1.

Tab. 4.1: Results from glow curve analysis comparison. The mean value for 6 TLDs was normalized to 1 Gy of the respective method. The coefficient of variation (CV) corresponds to the variation of 6 TLDs used at every dose level.

Dose [Gy]	**ROI**		**MAX**		**Deconvolution**	
	Mean [arb.unit]	**CV [%]**	**Mean [arb.unit]**	**CV [%]**	**Mean [arb.unit]**	**CV [%]**
0.2	0.20	2.6	0.20	2.7	0.19	4.4
0.5	0.50	3.0	0.50	2.7	0.50	2.8
1.0	1.00	3.1	1.00	3.0	1.00	3.0
1.5	1.54	2.8	1.54	3.3	1.50	3.6
1.8	1.97	2.8	1.98	2.8	1.92	1.7
2.0	2.16	2.1	2.16	2.2	2.13	3.6
2.2	2.32	3.3	2.33	3.6	2.25	3.9
3.0	3.31	2.7	3.33	2.6	3.08	0.9
5.0	5.95	2.2	5.99	2.5	5.25	1.8

The results obtained from ROI and MAX-method agree well with each other. The maximum difference between the approaches is 0.8 % at a dose of 5 Gy. Also coefficients of variation for both methods are comparable and lie between 2.1 and 3.6 %.

The glow curve deconvolution gave different results than ROI and MAX-method. The reason for this disagreement is a software issue with the GLOWFIT program. The outcome of the deconvolution depends strongly on the initial parameters, which have to be supplied by the user. To speed things up the software allows to store a set of initial values for a specific glow curve shape, for example TLD-100. These pre-defined values might not be optimal for every experimental glow curve in a large dataset and can lead to a mathematically optimal solution which isn't a good representation of the underlying physical principle. To improve the outcome of the deconvolution a unique set of initial parameters for every glow curve could be entered and

the deconvolution process should be supervised by the user to spot non-physical peak structures. However, such an approach is not feasible for large amounts of data. Another possible solution would be to record the glow curves with a lower heating rate. This would lead to less overlap of neighboring peaks and maybe to an improved deconvolution of the glow curves.

Due to the much higher effort the deconvolution is unfavorable compared to the MAX and ROI-method. The ROI-method was selected over the maximum method for all performed measurements. Since a larger area of the glow curve is involved for analysis, ROI-method is more robust against noise and the computational effort is still acceptable.

4.2 Individual sensitivity factors for TLD 100

The individual factors were calculated according to the procedure in section 4.1. The results are listed in the Tab. C1 of Appendix C. All sensitivity factors are in a range from 0.94 (TLD Nr. 29) to 1.06 (26) and show a coefficient of variation (defined in Eq. 4.6) between 0.09 (7) and 2.02 (37) (Fig. 4.1). Figure 4.2 shows the agreement of the three runs for the first 15 TLDs. The manufacturer of the TLDs, Thermo-Fisher Scientific, is stating values for sample to sample uniformity of ± 15 % and the repeatability of a single TLD to be below 2 %. The value for sample to sample uniformity is fulfilled by the investigated 48 TLDs with differences of about 12% between minimum and maximum individual sensitivity S_i. Liuzzi et. al. [46] reported similar results for uniformity (± 5 % around the mean value). The reproducibility of individual TLDs is for almost all TLDs within the 2% limit (maximum value 2.02 %). In this measurement not only TLD reproducibility but rather the reproducibility of the whole readout process was investigated. Therefore, also uncertainties from the reader and the annealing procedure are included and this value is higher than the reproducibility of the TLDs alone. Sadeghi et. al [47] also investigated the reproducibility of TLD-100 detectors and reported values of up to 3 %. The maximum value measured during this work was 2.02 %. The reproducibility strongly depends on the whole thermoluminescence procedure, including handling, annealing and readout, and can cause such a disagreement.

In all further measurements the TLD signals are corrected with the corresponding individual sensitivity factors. On average the CV of measurements was reduced by 50%. The impact of individual sensitivity factors on measurement are investigated in detail in the next section.

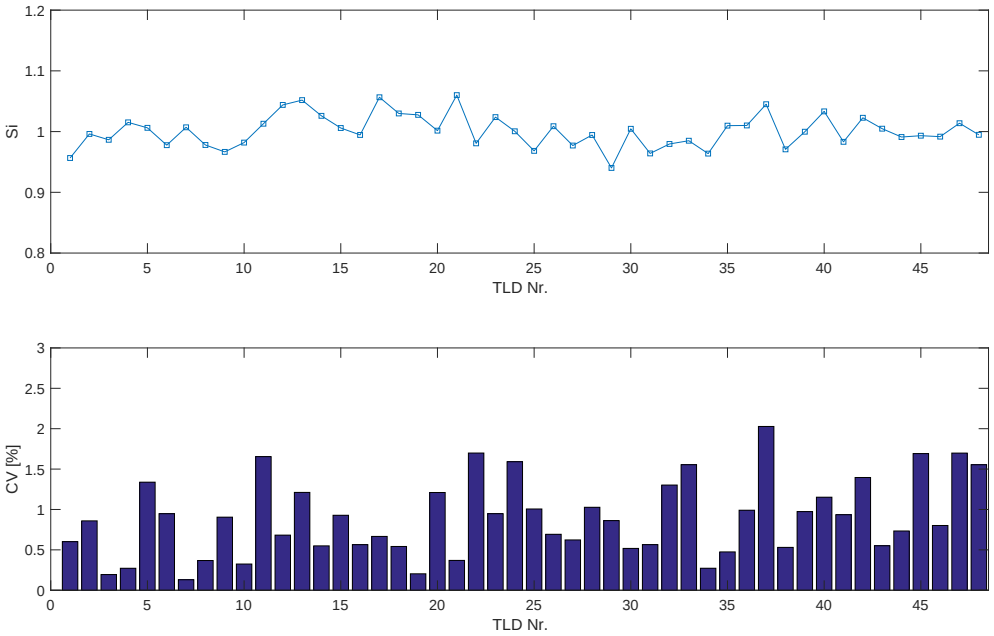

Fig. 4.1: Sensitvity factors (S_i) and respective coefficent of variation (CV) for every TLD.

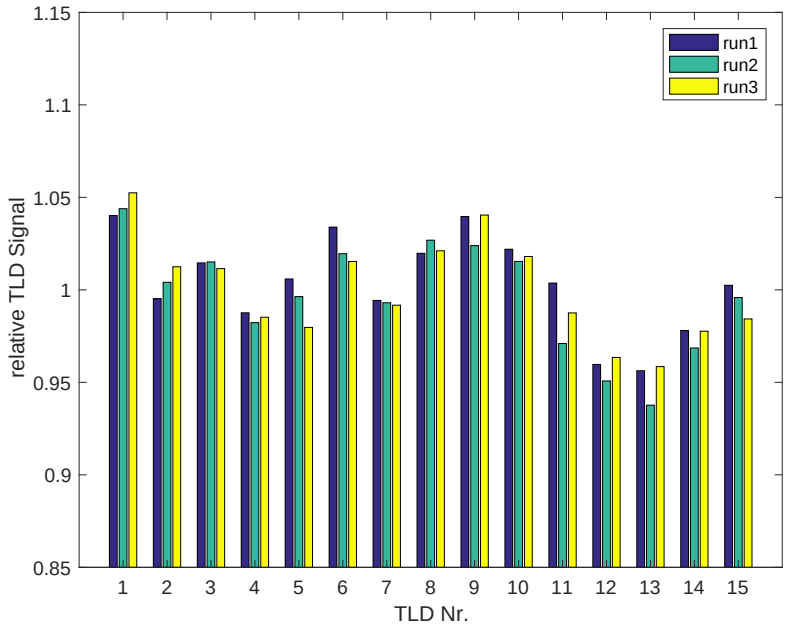

Fig. 4.2: TLD signals of TLD 1-15 for all 3 runs performed to determine the individual sensitivity factors.

4.3 Calibration in ^{60}Co

Measurements were performed, as described in section 4.2, to generate a calibration curve for TLDs, irradiated with a ^{60}Co unit. Table 4.2 shows the mean value for all TLDs investigated at

the respective dose level. Every TLD was corrected with the respective individual sensitivity factor. In Appendix C, Tab.C2 all individual TLD signals are listed.

Tab. 4.2: Results from calibration in a ^{60}Co beam. The mean value and standard deviation of all TLDs used at the respective dose levels are listed.

Dose [Gy]	**Mean**	**STD [%]**
0.20	1739670	1.2
0.50	4402291	0.3
1.00	8994388	0.9
1.50	13725036	1.0
1.83	16963979	0.8
1.99	18623971	0.8
2.19	20525375	2.2
2.99	28893548	2.3
4.98	52072879	2.2

As described in section 2.3, TLDs show linear behavior only up to a certain dose level, above that the response is supralinear. This is clearly visible in Fig. 4.3 where the TLD signal is plotted against the dose. The blue curve in Fig. 4.3 is a first order polynomial fitted to the low dose region (0.2-0.5 Gy) where linearity can be assumed. The orange curve is a second order polynomial in the form of:

$$M(D) = a \cdot D^2 + b \cdot D + c\,, \tag{4.1}$$

where D is the dose and M the TLD signal at dose D. Parameters a, b and c are fitting parameters.

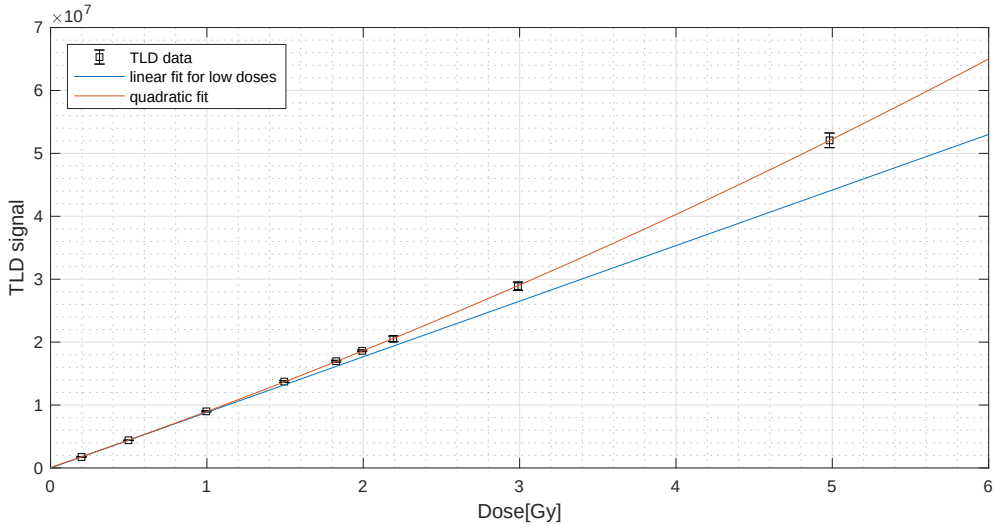

Fig. 4.3: Linear behavior of TLDs with linear fit for low doses and a 2nd order polynomial fit for full dose range

For ^{60}Co the parameters are:

$$a = 3.844 \cdot 10^5; b = 8.515 \cdot 10^6; c = 8.253 \cdot 10^4 \tag{4.2}$$

If Equation 9 is inverted we get a calibration curve for TLDs irradiated with ^{60}Co beams:

$$D(M) = \frac{-b + \sqrt{b^2 - 4a(c - M)}}{2a} \tag{4.3}$$

The quadratic fit and the calibration curve apply for the investigated dose region between 0.2 and 5 Gy. Especially for lower doses the quadratic fit would not be able to account for the existing linearity. The linearity index, defined in Eq. 3.7, quantifies the agreement between calibration dose and the TL detector's response. It indicates the sublinearity for values smaller than one, supralinearity for values larger than one and linearity for values equal to one. TLD-100, and LiF in general, is linear up to a dose of 1 Gy [42]. The transition value of linear and supralinear behavior varies with radiation type, readout procedure and annealing conditions [19].

For TLDs irradiated with ^{60}Co and the employed readout and annealing procedure, this transition value lies between 0.5 and 1 Gy. The linearity index (Fig. 4.4) was found to be 1.04 at 1.5 Gy, 1.06 (2 Gy), 1.09 (3 Gy) and increases up to 1.18 at the level of 5 Gy.

Impact of individual sensitivity factors

All measurements described above and all following measurements were corrected by the individual sensitivity factors listed in Tab. C1 (Appendix C). The obvious difference between the obtained results with and without applied individual sensitivity factors can be seen in Fig. 4.5. Table 4.3 gives an overview about standard deviations and their relative change before and after applying the corrections.

With applied individual sensitivity factors the standard deviation decreased on average by 50 percent. For high doses the decrease in standard deviation is more pronounced than for low doses. This might be an indication for a dose dependency of individual sensitivity factors. In the frame of this work the sensitivity factors were investigated at a dose level of 0.1 Gy.

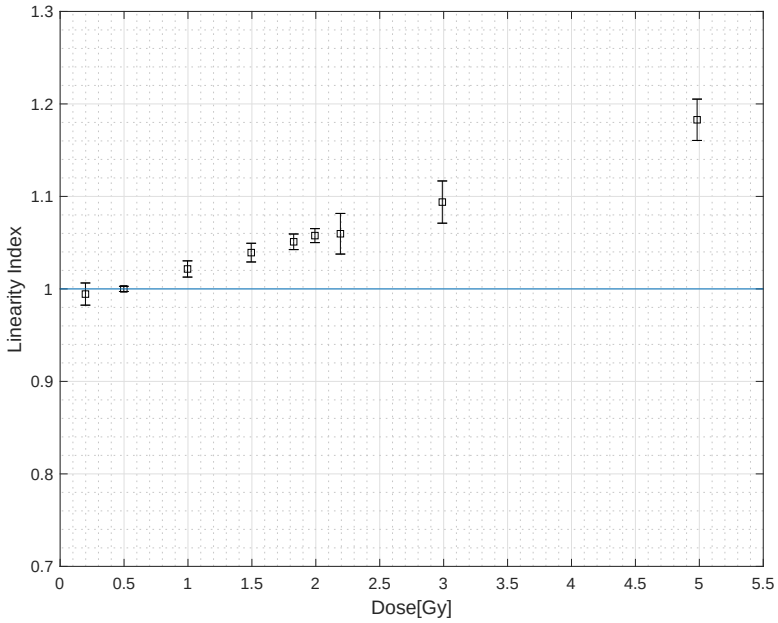

Fig. 4.4: Linearity index for TLD-100 calibrated in ^{60}Co beam.

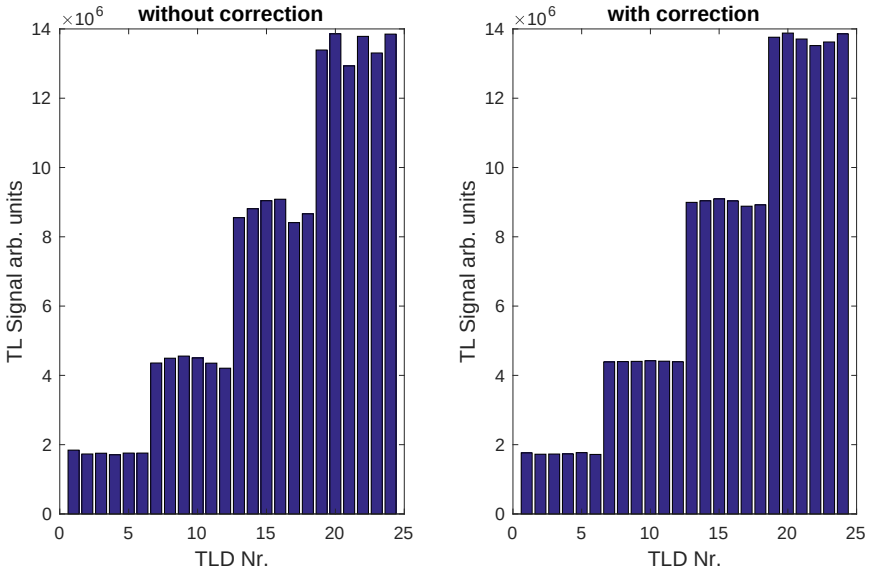

Fig. 4.5: Impact of individual sensitivity factors for the first four dose levels of ^{60}Co calibration. On the left without and on the right with individual sensitivity correction.

Tab. 4.3: Change of standard deviation when applying individual sensitivity factors to measurement results.

Dose [Gy]	rel. standard deviation		rel. change
	no corr.	with corr.	
0.2	2.6%	1.2%	-54.0%
0.5	3.0%	0.3%	-90.5%
1.0	3.1%	0.9%	-71.5%
1.5	2.8%	1.0%	-63.5%
1.8	2.8%	0.8%	-69.4%
2.0	2.1%	0.8%	-64.2%
2.2	3.3%	2.2%	-33.8%
3.0	2.7%	2.3%	-15.2%
5.0	2.2%	2.2%	-0.01%

4.4 Calibration in proton beams

Obtained data from the proton calibration was analyzed in the same way as for the ^{60}Co calibration. Table 4.4 shows the TLD results, which includes the mean value at a certain dose level and the standard deviation of five TLDs. The individual TLD signals for every TLD are given in Appendix C (Tab. C3). Polynomial functions were fitted to the data and the linearity index was calculated.

Tab. 4.4: Results from calibration of TLD-100 detectors in 179 MeV proton beams. The mean value and standard deviation of all TLDs used at the respective dose levels are listed.

Dose [Gy]	Mean	STD [%]
0.10	787741	1.7
0.20	1612769	0.5
0.49	4092179	1.6
0.98	8265021	1.3
1.47	12493292	0.9
1.76	15486067	1.6
1.96	17248528	1.4
2.16	19191579	0.5

The 1st and 2nd order polynomial functions are plotted in Fig. 4.6. The parameters of the quadratic fit for 179 MeV protons are

$$a = 3.844 \cdot 10^5; b = 8.515 \cdot 10^6; c = 8.253 \cdot 10^4 \tag{4.4}$$

for the equation

$$M(D) = a \cdot D^2 + b \cdot D + c. \tag{4.5}$$

The linearity index for protons shows similar behavior as in ^{60}Co (see Fig. 4.7). Supralinearity starts at a dose level below 1 Gy. Linearity index of 1.03 and 1.07 is achieved at the level of 1.5 and 2 Gy, respectively. For protons only doses up to 2.2 Gy were investigated, but a behaviour for higher doses comparable to ^{60}Co can be expected.

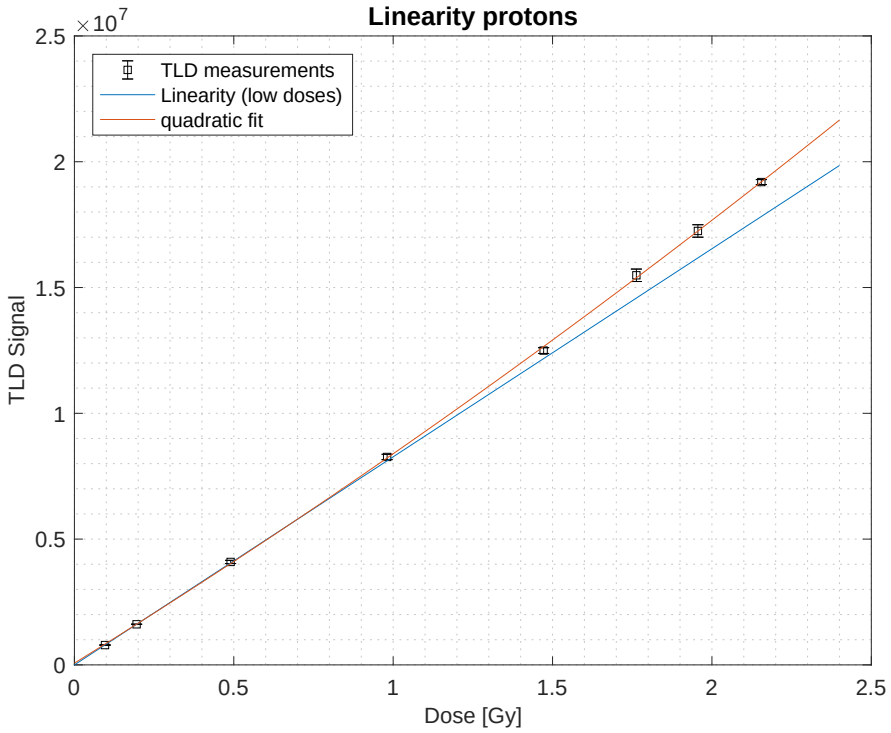

Fig. 4.6: Linear behavior of TLDs of type TLD-100 in proton radiation, linear fit (in blue) for low doses and a 2nd order polynomial fit (in red) for full investigated dose range.

Comparison of TLD response in ^{60}Co and proton beams

The term relative efficiency is often used when the response of TLDs in different radiation types is compared [44]. It is defined as

$$\eta = \frac{I_p/D_p}{I_\gamma/D_\gamma} \tag{4.6}$$

where I_p and D_p are thermoluminescent intensity and the corresponding absorbed dose of the investigated beam quality. In this case TLDs were calibrated proton beams at the energy of 179 MeV. I_γ and D_γ are the thermoluminescent intensities and the respective absorbed dose for a reference γ-radiation, in this case ^{60}Co. The relative intensity can than be plotted against the absorbed dose and the results are shown in Fig. 4.8.

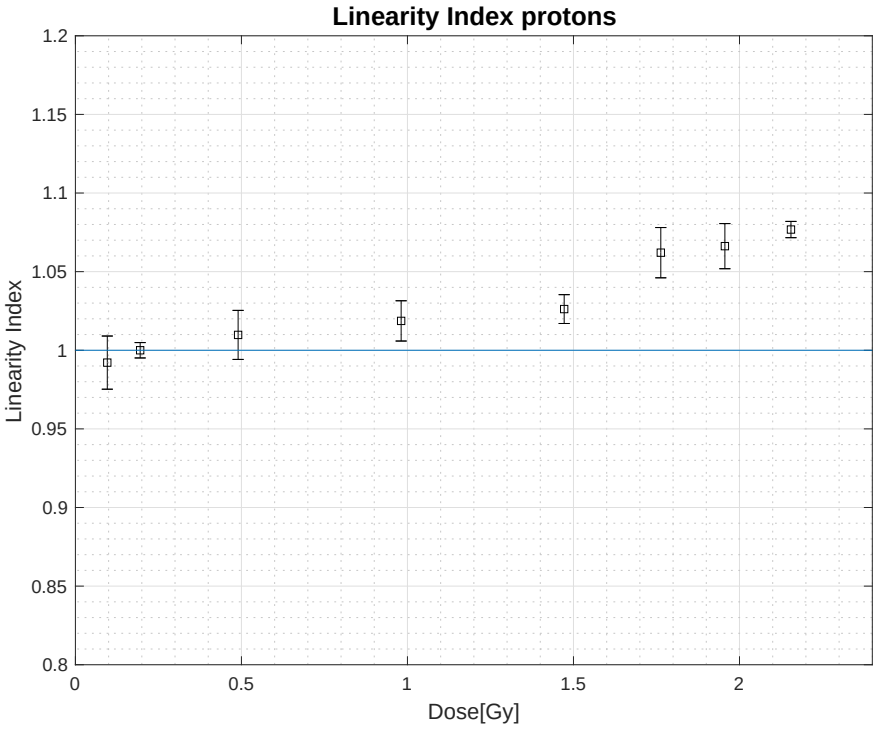

Fig. 4.7: Linearity index for TLD-100 disks irradiated with protons (179 MeV).

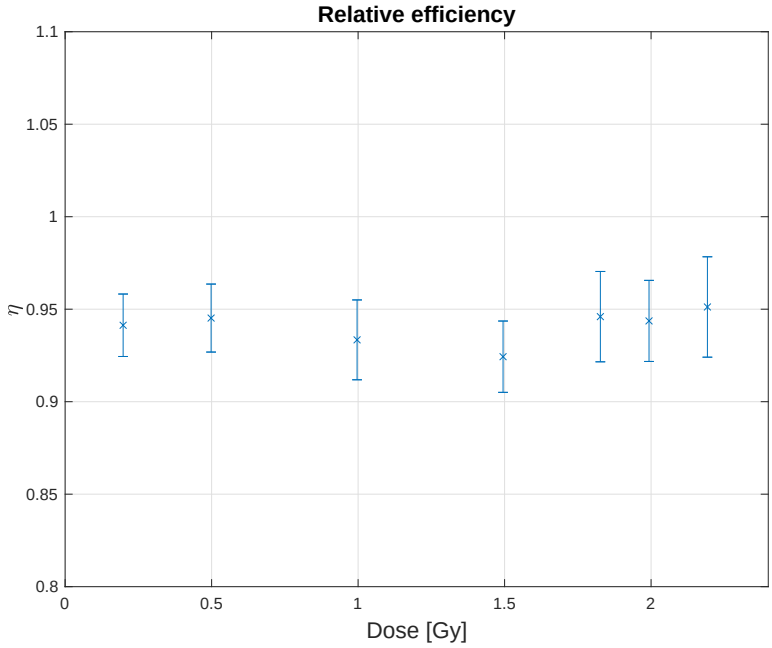

Fig. 4.8: Relative efficiency of TLD-100 detectors for ^{60}Co and proton radiation.

The relative efficiency, with a minimum value of 0.924 at 1.5 Gy and a maximum value of 0.951 (2.2 Gy), is almost constant over the investigated dose range from 0.2 to 2.2 Gy. The mean value lies at 0.94. The conclusion is that TLDs when irradiated with protons show 6% less response compared to TLDs irradiated in 60Co with the same dose. This difference is constant over the

investigated dose range. Figure 4.9 shows both calibration curves in comparison.

Sabini et. al [48] did not observe a difference in response for the different radiation qualities, but used lower proton beam energies of 62 MeV, compared to 179 MeV in this work. In ongoing measurements at MedAustron the energy dependence of TLDs in proton beams is investigated in detail.

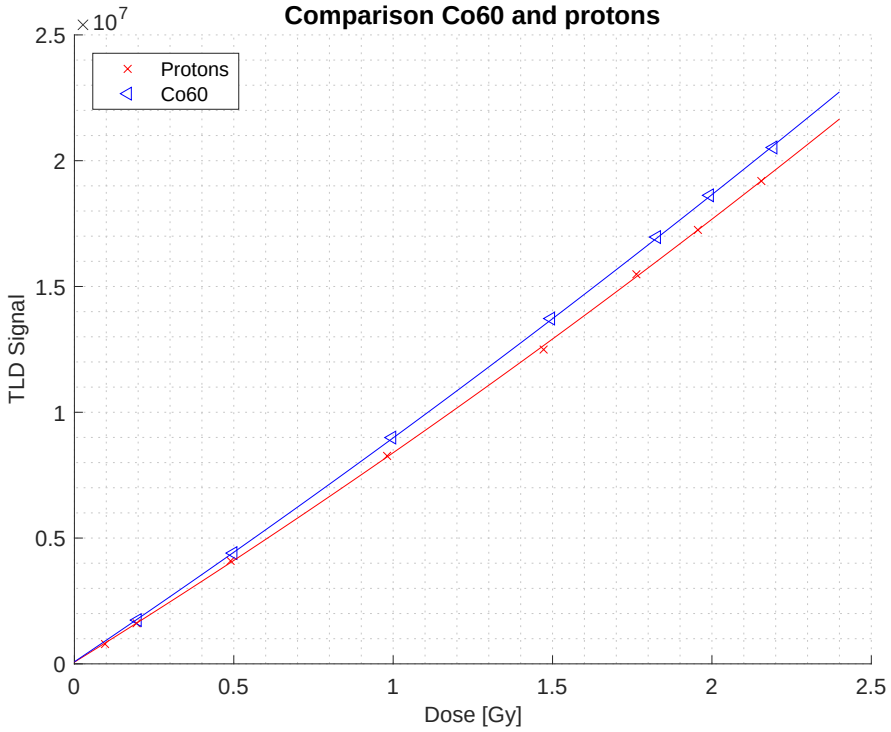

Fig. 4.9: Comparison of ^{60}Co and proton (179 MeV) calibration curves for TLD-100.

4.5 Spread-out Bragg peak irradiation with passive detectors

4.5.1 TLD results

In total 82 TLDs were irradiated at seven different depths in an SOBP with energies ranging from 69.5 to 133.8 MeV. The 82 TLDs were separated into two sets of 41 TLDs each. Both sets were irradiated at the same positions to gain information about the setup error. Table 4.5 summarizes the results. As described in section 3.6, the customized TLD phantom consists of seven plates, where the first plate has seven positions for TLDs. The following four plates are made for six TLDs and the last two plates can accommodate 5 detectors. More detailed results with TLD signals from every individual TLD are given in Appendix C (Tab. C4 and C5).

Tab. 4.5: TLD results from SOBP measurement for set 1 and 2. The mean value and standard deviation for both sets at the respective depth are listed.

WED [mm]	**Set 1**		**Set 2**	
	Mean	**CV [%]**	**Mean**	**CV [%]**
20.8	14450263	1.4	14427815	0.9
42.7	17024153	1.4	17063691	1.1
75.0	17235977	1.0	17224257	1.4
86.4	17157840	1.3	17450415	1.3
94.7	17166764	0.9	17381200	1.4
106.2	17229711	1.8	17293905	0.6
110.4	17148874	1.5	17061393	1.1

The use of individual sensitivity factors lead to an average standard deviation of 1.2 % and the maximum value does not exceed 1.8%. The results from two independent irradiations of the measurement setup (set 1 and set 2) agree very well. The largest difference between the two sets is about 1.5 % at a depth of 86.4 mm. This difference lies within the uncertainty of a TLD measurement. Results from both TLD sets were combined into one. Table 4.6 shows the doses for the individual sets as well as the average values of two measurement sets.

TLD calibrations

Two different calibration methods, acquired in proton beams, can be applied for TLDs. The first calibration, described in section 3.2, was performed in a single energy (179 MeV) proton beam. The calibration curve was obtained in the dose range between 0.1 and 2.2 Gy. The second calibration results from the SOBP irradiation. The Roos ionization chamber was positioned

within SOBP at the same place in the phantom as TLDs. An identical treatment plan was used to deliver uniform dose to the cylindrically shaped target (section 4.5, Plan design and TLD irradiation). The TLD signals were cross-calibrated to the Roos chamber value. Table 4.6 lists the TLD results from SOBP irradiation calibrated with two different methods. The reason for the two different calibration methods is that the monoenergetic calibration from chapter 3.2 was only done for 179 MeV and not for the lower energies that were used in the SOBP. For the cross-calibration with the ionization chamber we assume a linear dose gradient around the measured value. However, from the calibration curve (monoenergetic calibration) we already know that the curve shows globally a quadratic increase (Fig. 4.6). Hence the cross-calibration method is also valid only in a confined region around the calibrated dose. There the linear curve would be a valid approximation to the quadratic curve.

Tab. 4.6: Comparison of 179 MeV proton calibration and cross calibration for set 1, set 2 and a combination of both sets.

WED [mm]	**Dose IC cal. [Gy]**			**Dose 179MeV cal. [Gy]**		
	Set 1	**Set 2**	**Combined**	**Set 1**	**Set2**	**Combined**
20.8	1.61	1.60	1.61	1.66	1.66	1.66
42.7	1.89	1.89	1.89	1.93	1.94	1.94
75.0	1.92	1.91	1.92	1.96	1.95	1.96
86.4	1.91	1.94	1.92	1.95	1.98	1.96
94.7	1.91	1.93	1.92	1.95	1.97	1.96
106.2	1.92	1.92	1.92	1.95	1.96	1.96
110.4	1.91	1.89	1.90	1.95	1.94	1.94

At the first measurement position (depth of 20.82 mm) the cross-calibrated value is 3.5 % lower than the value from 179 MeV proton calibration (see Fig. 4.10). The remaining 6 depths show all a constant shift, of +2%, for the monoenergetic calibration. The increased difference in the first position is due to the fact that the cross-calibration is, as described above, only valid for a small dose interval around the calibration dose. The first measurement point is still in the dose build up, and since at this depth the dose is about 15% lower than in the SOBP, supralinearity has to be taken into account. For the remaining depths the constant shift of 2% indicates that there might be an energy dependence. A calibration for different energies or an energy correction factor has to be determined to get more accurate results without the need for a cross-calibration with an ionization chamber. The fact that the SOBP consists of an energy spectrum increases the complexity of such measurements and this aspect has to be considered if higher accuracy is required. The values from the cross-calibration are used for further discussion of measurement results.

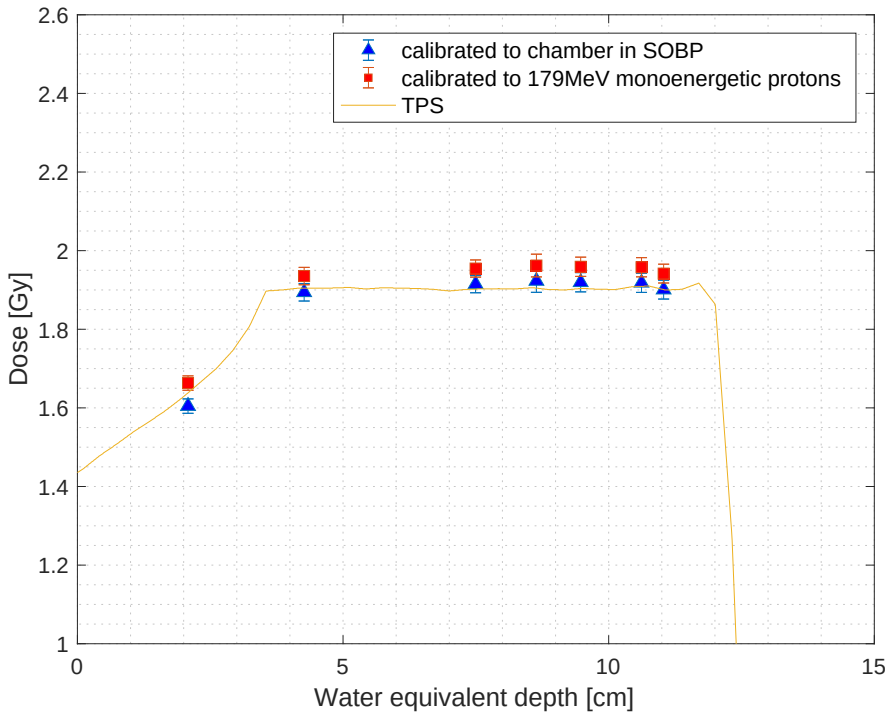

Fig. 4.10: Comparison of 179 MeV proton calibration (red squares) and cross-calibration with ionization chamber (blue triangles) for SOBP (8cm length, energies ranging from 69.5 to 133.8 MeV) measurement.

Measurements were performed with a Roos ionization chamber at depths of 43, 75 and 106 mm. The first depth was, as mentioned before, used for the TLD cross-calibration. All other TLDs from the SOBP irradiation were cross-calibrated with this value. The other two chamber measurements were acquired to measure the absolute dose at several positions along the SOBP. Moreover, the direct comparison between the ionization chamber and TLD results at multiple positions within SOBP was possible. At a depth of 75.0 mm ionization chamber and TLD show a difference of 0.8 % with IC measuring 1.90 Gy and TLDs 1.92 Gy. At 106.2 mm depth the relative difference is -0.1 % with an ionization chamber value of 1.92 Gy and and also 1.92 Gy for TLDs. At both depths the dose from ionization chamber and from TLDs lies well within the standard deviation of TLDs.

For this experimental setup, with an 8cm SOBP (energies ranging from 69.5 to 133.8 MeV) and TLDs positioned down to a residual range (distance to the 10 % dose level in the distal fall of of the SOBP) of about 11mm, no quenching was observed for TLDs. Reason for that might be the treatment of TLDs (annealing, read-out) or the experimental setup. These results are comparable to findings of Zullo et. al. [45], where measurements along a pristine Bragg-peak showed a deviation below 3% between TLDs and ionization chamber. In order to study the quenching effect in more detail, additional points would be beneficial, especially close to the

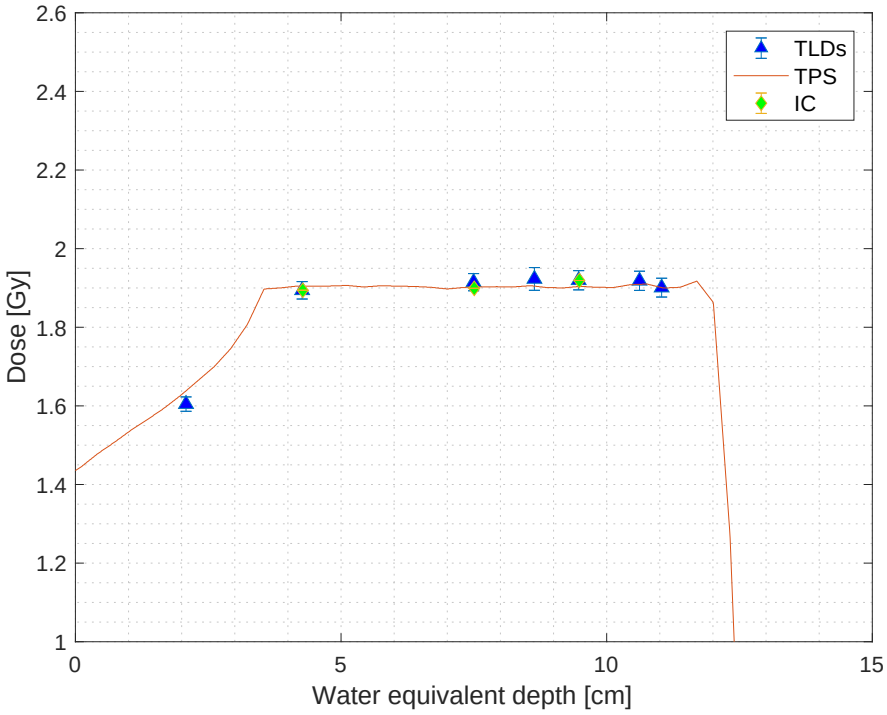

Fig. 4.11: TLD measurements (blue triangles) in a SOBP with energies ranging from 69.5 to 133.8 MeV and a length of 8 cm. TLD results from two irradiations with identical positioning were combined into one. Data from TPS (yellow line) and ionization chamber (green rhombus) is displayed for comparison.

distal fall-off, and MC simulations to estimate the LET.

4.5.2 Film results

Two sets of EBT-3 and EBT-XD films were irradiated under the same conditions as TLDs. Table 4.7 lists the dose values and the respective standard deviations for both film types. All dose values were calculated using available calibration data for both types of film at MedAustron. For the first six depths an averaged value from set 1 and 2 was calculated. For the remaining depths only a value from set 1 was available, and hence a standard deviation can only be calculated for the first six positions. The difference between the two measurements is more pronounced for films than for TLDs. An average difference of 3.3 % for EBT3 and 4.0 % for EBT-XD films was observed.

Figure 4.12 shows a comparison of EBT-3 and EBT-XD film results with results from ionization chamber measurment and the treatment planning system. For EBT3, the dose value at 43 mm depth agrees well with the ionization chamber (difference below 1 %) while the value for EBT-XD is 4.8 % higher than the chamber value. This difference might arise from the calibration used for

Tab. 4.7: Film results from SOBP (length of 8cm, energies ranging from 69.5 to 133.8 MeV) irradiation. The table lists the dose value and the standard deviation of EBT-3 and EBT-XD films at the respective irradiation depths. No standard deviation is given for last four films because only one irradiation was performed at this depths.

WED [mm]	EBT-3		EBT-XD	
	Dose [Gy]	STD [%]	Dose [Gy]	STD [%]
20.8	1.60	2.7	1.66	4.2
42.3	1.88	3.7	1.99	2.7
63.9	1.83	2.6	1.98	4.2
75.0	1.82	1.3	1.95	0.1
86.1	1.81	2.9	1.95	3.8
95.1	1.82	0.9	2.00	2.5
102.1	1.81	-	1.95	-
106.9	1.80	-	1.95	-
110.7	1.78	-	1.94	-
112.5	1.78	-	1.92	-

EBT-XD films. With increasing depth the dose measured by EBT3 films is decreasing. At a depth of 106 mm only 93.8 % of the dose from the ionization chamber is measured by the film. For EBT-XD this value lies at 101.8 % of the chamber value (compared to 104.8 % at the beginning of the SOBP). EBT3 film response decreases along the SOBP and the last measured point has a dose which is 6 % lower compared to the first measured point in SOBP. The dose decrease is present also for EBT-XD films, with the difference of 3 %. The decrease in the response along the SOBP is related to the signal quenching or detector saturation. Khachonkham et. al. [36] observed a similar value for EBT-3 quenching. For EBT-XD they measured an under-response of 8%, compared to 3% in this work. Both studies showed higher uncertainty for EBT-XD films when used in SOBPs.

4.5.3 Comparison of TLDs and films

Figure 4.13 shows a comparison of EBT-3 films, TLDs, ionization chamber and TPS. Because of the above descibed calibration issues EBT-XD films were not included. For films the difference between the two separately irradiated sets was a factor 3 to 4 higher than it was for TLDs. This results in larger uncertainty compared to TLDs. The agreement between TLDs and ionization chamber was better than for films. EBT3 and to a lesser extent also EBT-XD showed signs of quenching while for TLDs no quenching was observed in the investigated region. To summarize, different types of passive detectors were compared in SOBP. TLDs agree well with the ionization chamber and are suited for the measurements in the SOBP, since no quenching is present in the

investigated region. Films result in higher measurement error and show a continuing decrease in dose towards the end of SOBP related to quenching.

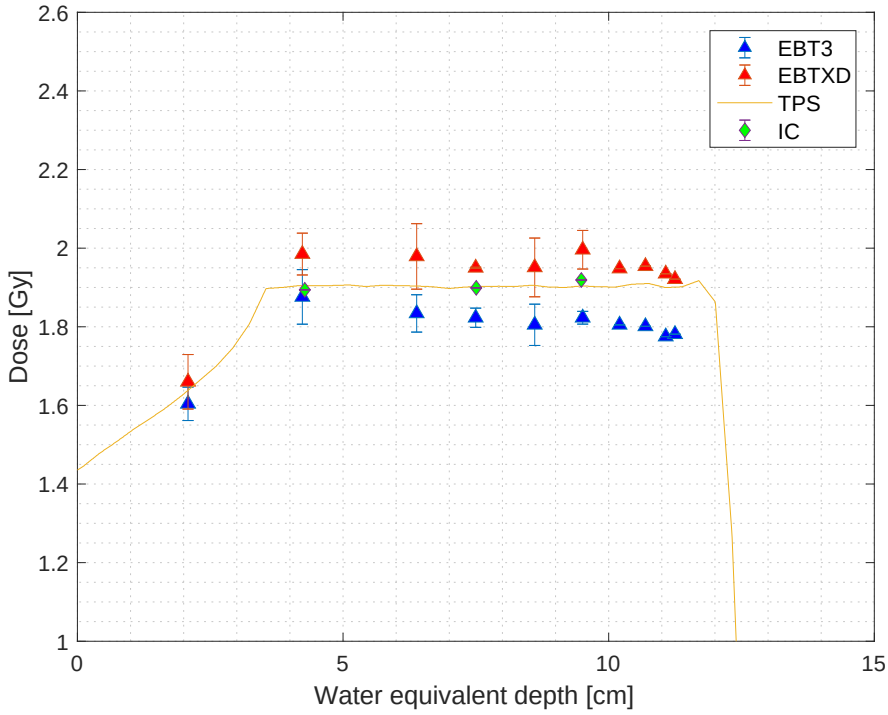

Fig. 4.12: Measurement in a SOBP with energies ranging from 69.5 to 133.8 MeV and a length of 8 cm. Results from EBT-3 films (blue triangles), EBT-XD films (red triangles), TPS (yellow line) and ionization chamber (green rhombus) are shown.

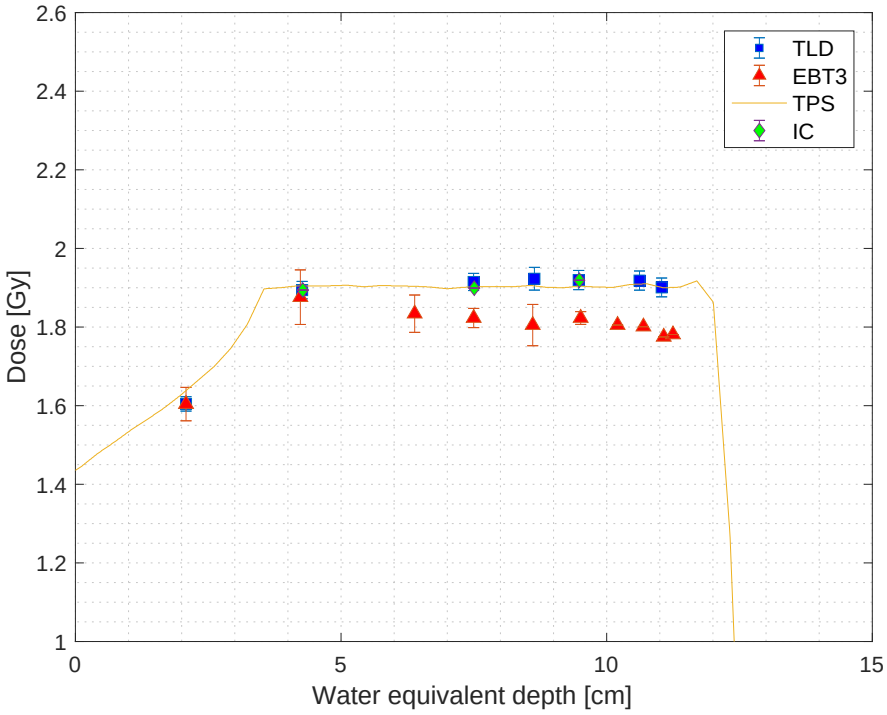

Fig. 4.13: Measurement in a SOBP with energies ranging from 69.5 to 133.8 MeV and a length of 8 cm. Results from TLD-100 (blue squares), EBT-3 films (red triangles) and TPS (yellow line) are shown.

5 Conclusion and Outlook

The aim of this work was to characterize and prepare a set of 192 new TLD-100 detectors in combination with the thermoluminescence equipment (TL-reader and annealing oven) for surface and in vivo dose measurements with proton beams at MedAustron.

Three different methods were applied to analyze the TL glow curve of the thermoluminescent detectors. MAX and ROI method led to similar results, whereas large deviations were observed in the method with a glow curve deconvolution. To get an improved outcome, a more detailed and work intensive approach for deconvolution, than the one used during this work, is needed. The ROI method was used in this work for all performed measurements.

Individual sensitivity factors were acquired repeatedly for 48 TLDs. The results showed that the vendor stated limits for sample-to-sample uniformity and reproducibility of individual TLDs are fulfilled for most of the TLDs. Significant improvement was demonstrated when TLD signals were corrected with individual sensitivity factors. The average standard deviation decreased by 50 %. This sensitivity correction, and as a consequence increased accuracy of TLDs, is crucial for a potential use as in vivo dosimeter in radiation oncology.

The detectors were calibrated in ^{60}Co beam and 179 MeV proton beams. Both calibrations showed a similar trend with supralinearity starting between 0.5 and 1 Gy. Supralinearity index of 1.06 and 1.07 was obtained at the dose level of 2 Gy for ^{60}Co and proton beams, respectively. Detector signals in proton radiation were by 6 % smaller in comparison with that of ^{60}Co radiation.

Reasonable results were obtained using the proton calibration for TLD measurements in the SOBP. TLD calibration with 179 MeV proton beams, showed a constant shift of about 2 % when compared to cross-calibration with ionization chamber . Since the SOBP (69.5 to 133.8 MeV) consisted of proton beams with energies lower than 179 MeV, this might indicate an energy dependence of TLDs. Energy dependence of TLDs is currently being investigated in ongoing measurements of calibration curves using various energies at MedAustron.

The in-house built TLD slab phantom was used to obtain the response of TLDs in a SOBP. The customized phantom allows positioning of 41 TLDs in seven depths of the Bragg curve

simultaneously. The averaged standard deviation of TLD signals from all seven depths was at 1.2%. TLD signals were corrected with corresponding individual sensitivity factors. For comparison, the averaged standard deviation obtained without the correction factors would be 3.3 %. For the measured range no LET dependence of TLDs was observed in the SOBP. EBT3 and EBT-XD films were irradiated under same conditions and compared to TLDs. A higher variation for the two film sets and presence of LET-quenching along the SOBP (6 % for EBT3, 3 % for EBT-XD) was observed. More measurement points, closer to the distal fall-off and accompanying LET-simulations would give more insight on TLD behavior in this region. Measurements in this direction are already in progress.

The presented results demonstrate the potential of using the investigated TLDs, of type TLD-100, in surface and in-vivo dosimetry. However, the consistency in the process of using and treating the TLDs is a very crucial aspect. The lengthy procedure of annealing and readout should be followed as recommended, since any deviation will have an impact on the data. The change will be recognized only after the measurement and cannot be corrected backwards. This implies regular quality assurance of all involved parts has to be performed to ensure properly working TLDs. The use of TLDs is rather time consuming and if TLDs are not regularly used this might be an argument against them. As an alternative OSLDs or diode detectors could be used for in-vivo dosimetry.

Appendix

Appendix A

Appendix A contains all drawings with dimensions of the in-house modified RW3 TLD slabs.

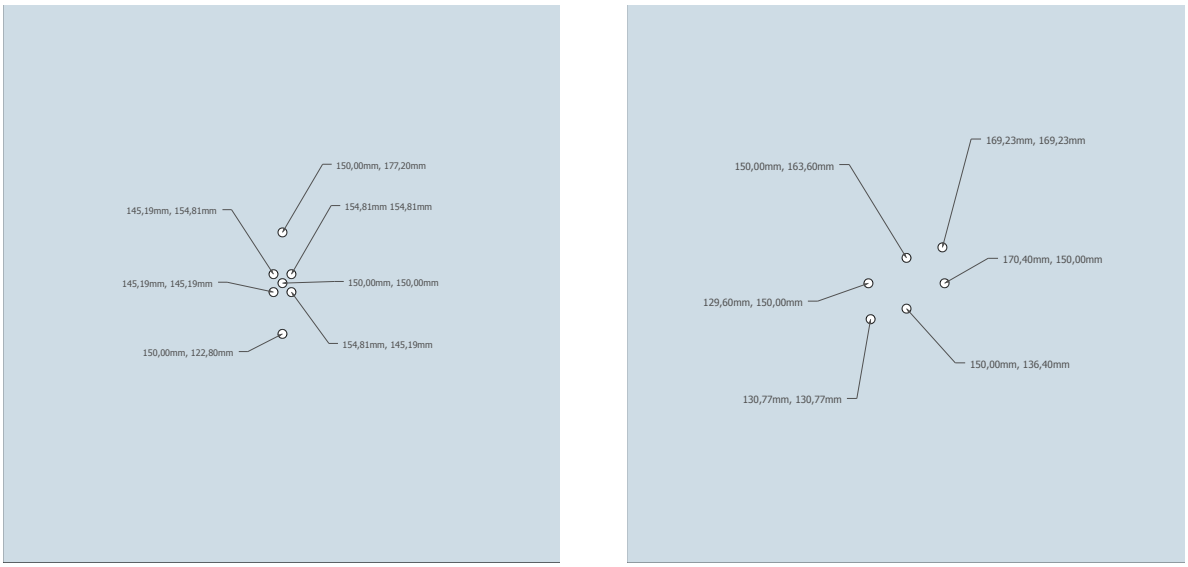

(a) **(b)**

Fig. A1: Distribution of inserts for TLDs of a) plate 1 and b) plate 2

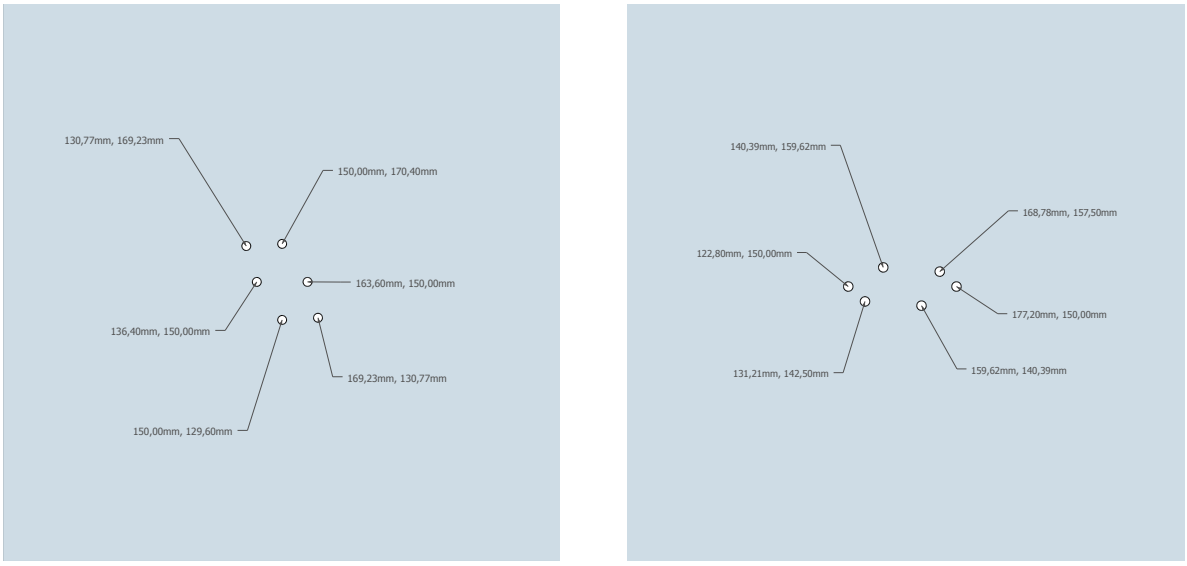

(a) **(b)**

Fig. A2: Distribution of inserts for TLDs of a) plate 3 and b) plate 4

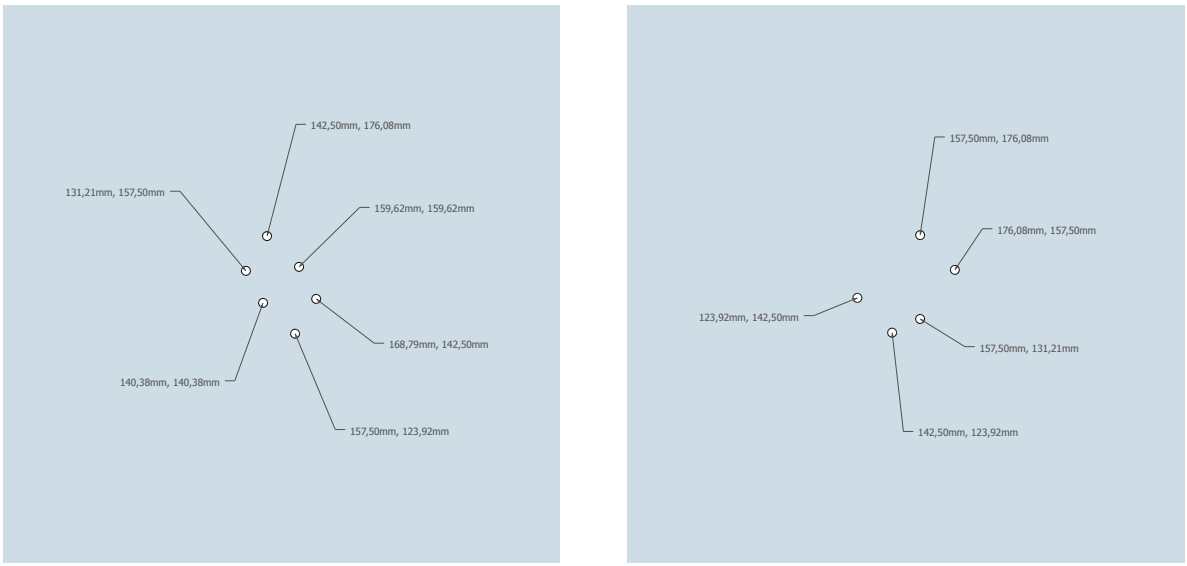

(a) **(b)**

Fig. A3: Distribution of inserts for TLDs of a) plate 5 and b) plate 6

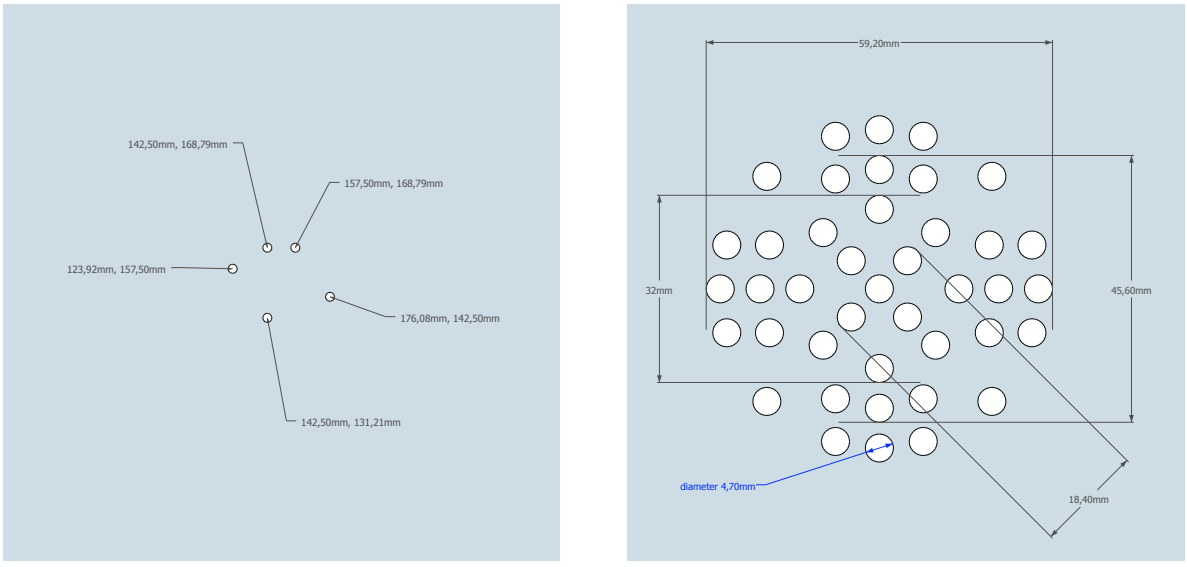

(a) **(b)**

Fig. A4: a)Distribution of inserts for TLDs of plate 7 and b) overall dimensions

Appendix B

The below listed scripts were developed with MATLAB software suite to analyze and plot the output data from the Risø-DA20 TL/OSL reader. The reader is equipped with the Analyst software, which can also be used to analyze glow-curve data. However the Analyst software is meant for a quick analysis an not for a comprehensive evaluation. The Analyst software has the capability to export data from the reader into simple .txt files.

readTLD.m

In a .txt file from the Analyst software up to 48 glow curves are stored. The script readTLD.m opens this .txt file and stores the glow-curve data into a matrix where the number of rows is equal to the recorded datapoints and the number of columns equal is to the recorded glow curves.

```
function [data,nrdatapoints,nrofmeas] = readTLD(filename)
%reading riso txt-file

%input: filename
%outputs:
%data: matrix with glowcurve data, every column responds to one glowcurve

%opening file with specified name
filename;
fileID = fopen(filename);
C=textscan(fileID,'%s','Delimiter',',');

%find out selected entries
i=1;
while (isempty(str2num(C{1,1}{i}))==1)  %find out number of columns
    i=i+1;
end
col=i-1;
C=C{1,1};

%find out nr. of datapoints

[rn,cn]=find(strcmp('Num. Points',C));
```

```
24 nrdatapoints=C{col+rn};
25 nrdatapoints=str2num(nrdatapoints);
26
27 %find out nr. of measurements
28
29 s=size(C);
30 s=s(1);
31 nrofmeas=(s-col)/(nrdatapoints+col);
32
33 %make 1 column for each measurement
34
35 for k=1:nrofmeas
36     for l=1:nrdatapoints
37         ind=2*col+(k-1)*(nrdatapoints+col)+l;
38         data(k,l)=str2num(C{ind});
39     end
40 end
41
42 data=transpose(data);
43
44 end
```

integralTLD.m

The script integralTLD.m is used to sum up channels around the maximum value of the glow-curve. The user can set the upper and lower boundary. This script was used to calculate the ROI-dose determination method (see section 4.4)

```
1 function [integral] = integralTLD(data,boundaryl,boundaryu)
2 %integrating tld glowcurve data from readTLD
3
4 %inputs:
5 %data: output from readTLD
6 %boundaryl: lower boundary for integration e.g. 10 for 10 channels below
      maximum
7 %boundaryu: higher boundary for integration e.g 10 for 10 channels above
      maximum
8
```

```
%output:
%integral: results for every glowcurve in data

s=size(data);
boundaries=[boundaryl,boundaryu];

for i=1:s(2)
   m(i)=max(data(:,i));
%    halfmax=find(data(:,i)==m(i)/2)
end

for i=1:s(2)
    m(i)=max(data(:,i));
    f=find(data(:,i)==m(i));
    tofmax(i)=f(1);
    datax=data(:,i);
    integral(i)=sum(datax(tofmax(i)-boundaries(1):tofmax(i)+boundaries(2)));
end
end
```

maxTLD.m

MaxTLD.m is used for dose determination when only the maximum value is used for it.

```
function [maxval] = maxTLD(data)
%integrating tld data
%inputs:
%data: output from readTLD
%outputs:
%maxval: maximum value of every glowcurve
s=size(data);

for i=1:s(2)
   maxval(i)=max(data(:,i));
end

end
```

Appendix C

Appendix C contains tables with extended TLD results from inidvidual sensitvity factor determination and SOBP irradiation.

Tab. C1: Results from individual sensitivity factor determination

TLD Nr.	**TLD Signal**				**Std** [%]	S_i
	1st cycle	2nd cycle	3rd cycle	Mean		
1	574004	575766	581485	577085	0.7	0.957
2	549204	553820	559395	554140	0.9	0.996
3	559876	559891	558835	559534	0.1	0.986
4	544996	541778	544321	543698	0.3	1.015
5	555089	549537	541290	548639	1.3	1.006
6	570545	562341	560978	564621	0.9	0.978
7	548679	547720	547917	548105	0.1	1.007
8	562730	566373	564168	564424	0.3	0.978
9	573690	564748	574840	571093	1.0	0.967
10	563945	560042	562466	562151	0.4	0.982
11	553854	535571	545613	545013	1.7	1.013
12	529580	524406	532317	528768	0.8	1.044
13	527704	517182	529573	524820	1.3	1.052
14	539693	534234	540153	538027	0.6	1.026
15	553190	549279	543812	548760	0.9	1.006
16	553891	552140	559110	555047	0.7	0.994
17	524290	524102	518946	522446	0.6	1.057
18	534750	533388	539804	535981	0.6	1.030
19	536781	537986	536757	537175	0.1	1.028
20	558778	546471	548271	551173	1.2	1.002
21	519081	519638	523381	520700	0.5	1.060
22	572443	553049	563417	562970	1.7	0.981
23	536394	544666	536364	539141	0.9	1.024
24	555432	557542	542344	551773	1.5	1.001
25	568401	576053	565829	570094	0.9	0.968
26	551367	544900	545108	547125	0.7	1.009
27	562894	568620	563357	564957	0.6	0.977
28	556182	559670	549441	555098	0.9	0.994
29	581297	588565	591564	587142	0.9	0.940
30	546122	550065	552190	549459	0.6	1.005
31	571272	575811	570623	572569	0.5	0.964
32	557337	571315	561868	563507	1.3	0.980
33	550582	566737	564140	560486	1.6	0.985
34	573564	573147	571491	572734	0.2	0.964
35	545886	549077	544917	546627	0.4	1.010
36	540375	547591	551507	546491	1.0	1.010
37	515967	534567	534377	528304	2.0	1.045
38	566887	571693	567276	568619	0.5	0.971
39	554374	545602	556407	552128	1.0	1.000
40	529581	531301	541807	534230	1.2	1.033
41	566775	560684	556960	561473	0.9	0.983
42	531051	542924	545337	539771	1.4	1.023
43	549168	545951	552938	549352	0.6	1.005
44	554713	561279	554880	556957	0.7	0.991
45	554659	546565	566282	555835	1.8	0.993
46	561618	553091	555143	556617	0.8	0.992
47	546895	533986	552778	544553	1.8	1.014
48	552474	564222	548321	555006	1.5	0.995
Mean	551835	551564	552502	551967	0.9	1.00

Tab. C2: Results from linearity measurements in ^{60}Co

Dose [Gy]	TLD 1	TLD 2	TLD 3	TLD 4	TLD 5	TLD 6	Mean	STD [%]
0.20	1762673	1724843	1729972	1733152	1768771	1718608	1739670	1.2
0.50	4388104	4397003	4404895	4421444	4409712	4392587	4402291	0.3
1.00	8994197	9038112	9094308	9034879	8883741	8921090	8994388	0.9
1.50	13760686	13880322	13708989	13518709	13623462	13858046	13725036	1.0
1.83	17110268	17126315	16777709	16994080	16948487	16827017	16963979	0.8
1.99	18591354	18417169	18852368	18617317	18594302	18671315	18623971	0.8
2.19	20610795	20419763	19680774	20662510	20908943	20869464	20525375	2.2
2.99	28455773	28572768	29652104				28893548	2.3
4.98	52872783	52608122	50737732				52072879	2.2

Tab. C3: TLD data of linearity measurements with protons

Dose [Gy]	TLD 1	TLD 2	TLD 3	TLD 4	TLD 5	Mean	STD [%]
0.10	773383	795690	780017	806660	782954	787741	1.7
0.20	1619701	1602264	1606861	1619820	1615199	1612769	0.5
0.49	4152048	4166652	4053122	4021189	4067883	4092179	1.6
0.98	8204259	8441508	8286905	8199331	8193103	8265021	1.3
1.47	12559914	12552435	12564010	12495725	12294375	12493292	0.9
1.76	15442382	15662037	15594244	15072901	15658771	15486067	1.6
1.96	17572037	16919485	17238102	17383077	17129937	17248528	1.4
2.16	19194031	19183290	19311195	19038301	19231077	19191579	0.5

Tab. C4: TLD results from SOBP set 1

WED [mm]	TLD 1	TLD 2	TLD 3	TLD 4	TLD 5	TLD 6	TLD 7	Mean	CV [%]
20.8	14880625	14283998	14359270	14362715	14516434	14387484	14361315	14450263	1.4
42.7	16668488	17173688	16796903	17133311	17245198	17127327		17024153	1.4
75.0	17346945	17514454	17269854	17124577	17056062	17103971		17235977	1.0
86.4	17272103	17203998	16888096	16878390	17355283	17349171		17157840	1.3
94.7	17309627	17269639	17011355	17306485	17114122	16989354		17166764	0.9
106.2	17199326	17412923	17651035	16989275	16895996			17229711	1.8
110.4	17154138	16786000	17082817	17225092	17496323			17148874	1.5

Tab. C5: TLD results from SOBP set 2

WED [mm]	TLD 1	TLD 2	TLD 3	TLD 4	TLD 5	TLD 6	TLD 7	Mean	CV [%]
20.8	14543003	14412071	14260345	14466578	14320209	14641317	14351179	14427815	0.9
42.7	16778351	17219977	17091768	17160156	16916494	17215400	-	17063691	1.1
75.0	17524919	17315549	17176407	17286936	16815840	17225890	-	17224257	1.4
86.4	17557588	17772690	17535092	17276497	17414161	17146460	-	17450415	1.3
94.7	17301308	17165952	17314370	17172971	17559883	17772718	-	17381200	1.4
106.2	16896167	16911838	17148765	17012838	17337359	-	-	17061393	11
110.4	17176396	17311374	17251158	17454844	17275751	-	-	17293905	0.6

Appendix D

QA and maintenance procedures

Regular quality assurance and maintenance of all involved parts is necessary to enable a proper working thermoluminescence dosimetry system (dosimeters, reader, oven). Based on experiences within the scope of this work, recommendations for the used system at MedAustron are given.

Detectors

Every time TLDs are used a visual inspection should be carried out. If damage or dirt is clearly visible TLDs should be excluded from measurements. To prevent any damage or contamination TLDs should be stored in an enclosed tray and proper tweezers should be used. If TLDs still get dirty during measurements, annealing or readout, cleaning instructions for TLDs are available. For TLD-100, the manufacturer recommends cleaning with methanol (analytical grade). Cleaning might interfere with the labeling and should only be done if really necessary.

Due to contamination and wear of detectors the sensitivity might change. Hence it is necessary to check the individual sensitivity factors regularly. Currently at MedAustron these factors are obtained before or after every measurement to ensure the best possible sensitivity correction. If in the future, stable TLD sensitivity is observed, the frequency of the sensitivity check can be adapted accordingly.

TLD-reader

The inside of the Risø TLD-reader has to be cleaned regularly to ensure proper operation. The use of chemicals for cleaning should be prevented because evaporation inside the reader can influence the TLD readings. Dust can be removed by a moist cloth or a small vacuum cleaner. To ensure proper closing of the lid, the black rubber seal should be covered with a thin layer of vacuum grease. Sample holders (cups and disks shown in Fig. 2.5) should be cleaned or exchanged if dirt or contamination is visible. It is recommended to clean the sample holders with soap water and carefully rinse them afterwards with water. Since sample holders are heated up to 400°C no residues of detergents should be present on the holders. A dry run (without

detectors) should be performed in the reader after cleaning the holders

The PMT inside the reader is covered by a protective quartz window and should be cleaned with a dry lens cleaning wipe if any pollution is visible. Any cleaning of the reader might influence the readout performance and should be followed by a determination of individual sensitivity factors for TLDs. Additional information about maintenance for the Risø TLD reader can be found in [30].

TLD-oven

During annealing, TLDs are placed on a metal tray. This tray has to be inspected and cleaned. The high temperatures inside the oven can lead to unwanted reactions between residues and TLDs. It's advisable for consistency to place TLDs always on the same position within the tray.

List of Figures

List of Tables

Bibliography

[1] K. Yamoah and P. Johnstone. Proton beam therapy: clinical utility and current status in prostate cancer. *OncoTargets and Therapy*, 9:5721–5727, 2016.

[2] Ervin B. Podgorsak. *Radiation Physics for Medical Physicists.* Springer, 2010.

[3] E. Stancu, E. Badita, F. Scarlat, and A. Scarisoreanu. Evaluation of quality factor for clinical proton beams. *Romanian Reports in Physics*, 66(1):192–199, 2014.

[4] S. Meroli. Multiple scattering for particles in matter. Webpage.

[5] Rui Zhang and Wayne D Newhauser. Calculation of water equivalent thickness of materials of arbitrary density, elemental composition and thickness in proton beam irradiation. *Physics in Medicine and Biology*, 54(6), 2009.

[6] Wayne D Newhauser and Rui Zhang. The physics of proton therapy. *Physics in Medicine and Biology*, 60, 2015.

[7] C.-M. Charlie Ma and Tony Lomax, editors. *Proton and Carbon Ion Therapy.* CRC Press, 2013.

[8] IAEA Tech Report. Absorbed Dose Determination in External Beam Radiotherapy. Technical Report 398, International Atomic Energy Agency, 2000.

[9] Ervin B. Podgorsak. *Radiation Physics for Medical Physicists, Third Edition.* Graduate Texts in Physics. Springer, 2016.

[10] Hanno Krieger. *Grundlagen der Strahlenphysik und des Strahlenschutzes*, volume 4. Springer Spektrum, 2012.

[11] Hugo Palmans and Stanislav M. Vatnitsky. Beam monitor calibration in scanned light-ion beams. *Medical Physics*, 43(11):5835–5847, 2016.

[12] D Nichiporov, V Kostjuchenko, JM Puhl, DL Bensen, MF Desrosieres, DE Dick, WL McLaughlin, T Kojima, BM Coursey, and S Zink. Investigation of applicability of alanine and radiochromic detectors to dosimetry of proton clinical beams. *Applied Radiation and Isotopes*, 46(12), 1995.

[13] G. Mierzwinska, B. Michalec, I. Oglodek, B.Petelenz, and M.P.R. Waligorski. Alanine/EPR dosimetry as a potential tool for quality assurance in proton beam radiotherapy. *Romanian Reports in Physics*, 66(1):54–60, 2014.

[14] Kirby D, Green S, Palmans H, Hugtenburg R, Wojnecki C, and Parker D. LET dependence of GafChromic films and an ion chamber in low-energy proton dosimetry. *Physics in Medicine and Biology*, 55(2), 2010.

[15] C.M. Sunta. *Unraveling Thermoluminescence*. Springer, 2015.

[16] Reuven Chen and Stephen W S McKeever. *Theory of Thermoluminescence and Related Phenomena*. World Scientific, 1997.

[17] J.T. Randall and M.H.F. Wilkins. Phosphorescence and electron traps I. The study of trap distributions. *Proceedings of the Royal Society*, 184(999), November 1945.

[18] E. Lilley and S.W.S. McKeever. On the order of kinetics for thermoluminescence in LiF (TLD-100). *Journal of Physics D: Applied Physics*, 16(2), 1983.

[19] Tomas Kron. Thermoluminescence dosimetry and its applications in medicine–Part 1: Physics, materials and equipment. *Australasian physical and engineering sciences in medicine*, 1995.

[20] Alessio Parisi, Olivier Van Hoey, Patrice Megret, and Filip Vanhavere. The influence of the dose assessment method on the LET dependence of the relative luminescence efficiency of LiF:Mg,Ti and LiF:Mg,Cu,P. *Radiation Measurements*, 98:34–40, 2017.

[21] R. Chen and P.L. Leung. Nonlinear dose dependence and dose-rate dependence of optically stimulated luminescence and thermoluminescence. *Radiation Measurements*, 33:475–481, 2001.

[22] Georg Wilding. Linearity and residual dose correction of a LiF:Mg,Ti thermoluminescence dosimeter. Master thesis, February 2015.

[23] Accelerator Complex Study Group. Proton-Ion Medical Machine Study (PIMMS) Part 1. Technical report, Cern, 1999.

[24] Markus Stock, Dietmar Georg, Alexander Ableitingr, Andrea Zechner, Alexander Utz, Marta Mumot, Gabriele Kragl, Johannes Hopfgartner, Joanna Gora, Till Böhlen, Loic Grevillot, Peter Kuess, Phil Steininger, Heinz Deutschmann, and Stanislav Vatnitsky. The technological basis for adaptive ion beam therapy at MedAustron: Status and outlook. *Zeitschrift für Medizinische Physik*, 2017.

[25] Narayan Sahoo. In vivo Dosimetry for proton therapy. Presentation AAPM Summer School, 2015.

[26] Sonja Dieterich, Eric Ford, Dan Pavord, and Jing Zeng. *Practical Radiation Oncology Physics*. Elsevier, 2016.

[27] Harald Paganetti. Range uncertainties in proton therapy and the role of Monte Carlo simulations. *Physics in Medicine and Biology*, 57(11), 2012.

[28] P. Bilski, M. Budzanowski, W. Hoffmann, A. Molokanov, P. Olko, and M.P.R. Waligorski. Investigation of Efficiency of Thermoluminescence Detectors for Particle Therapy Beams. *Radiation Protection Dosimetry*, 70(1-4):501–504, 1997.

[29] Claudio Furetta. *Handbook of Thermoluminescence*. World Scientific, 2003.

[30] DTU Nutech. *Guide to the "The Risø TL/OSL Reader"*, August 2015.

[31] Kristina Jørkov Thomsen. *Optically Stimulated Luminescence Techniques in Retrospective Dosimetry using Single Grains of Quartz extracted from Unheated Materials*. PhD thesis, Risø National Laboratory, Roskilde, Denmark, February 2004.

[32] Markus Demel. Thermoluminescence-Annealing. Project thesis, 2018.

[33] Adrian Thummerer. Characterisation of Thermoluminescent Dosimeters at MedAustron. Project thesis, 2017.

[34] PTW-Freiburg. *Service Manual, TLD Annealing Oven*.

[35] Ralf Dreindl, Dietmar Georg, and Markus Stock. Radiochromic film dosimetry: Considerations on precision and accuracy for EBT2 and EBT3 type films. *Zeitschrift für Medizinische Physik*, 24:153–163, 2014.

[36] Suphalak Khachonkham, Ralf Dreindl, Gerd Heilemann, Wolfgang Lechner, Hermann Fuchs, Hugo Palmans, Dietmar Georg, and Peter Kuess. Characteristic of EBT-XD and EBT3 radiochromic film dosimetry for photon and proton beams. *Physics in Medicine and Biology*, 2018.

[37] PTW-Freiburg. *User Manual, Ionization Chamber Type 30010, 30011, 30012, 30013*, 03 2013.

[38] PTW-Freiburg. *User Manual, Ionization Chamber Type 34001*, 01 2016.

[39] PTW-Freiburg. *User Manual, UNIDOS webline*, 08 2014.

[40] PTW-Freiburg. *Instruction Manual, RW3 Slab Phantom T29672 and T40006.1.1001*, 02 2011.

[41] M. Puchalska and P. Bilski. GlowFit—a new tool for thermoluminescence glow-curve deconvolution. *Radiation Measurements*, 41(6):659–664, July 2006.

[42] Yigal Horowitz. *Microdosimetric Response of Physical and Biological Systems to Low- and High-LET Radiations*. Elsevier Science, 2006.

[43] P.Bilski, M. Sadel, J.Swakon, and P.Olko. Investigation of the relatitve efficiency of thermoluminescent detectors to protons at the IFJ pan Krakow. Presentation, WRMISS-19, September 2004.

[44] P. Bilski. Calculation of the relative efficiency of thermoluminescent detectors to space radiation. *Radiation Measurements*, 46:1728–1731, 2011.

[45] John R. Zullo, Rajat J. Kudchadker, X.Ronald Zhu, Narayan Sahoo, and Michael T. Gillin. LiF TLD-100 as a dosimeter in high energy proton beam therapy- can it yield accurate results? *Medical Dosimetry*, 35(1):63–66, 2010.

[46] R. Liuzzi, F. Savino, V. D'Avino, M. Pugliese, and L. Cella. Evaluation of LiF:Mg,Ti (TLD-100) for Intraoperative Electron Radiation Therapy and Quality Assurance. *PLOS One*, 2015.

[47] M. Sadeghi, S. Sina, and R. Faghihi. Investigation of LiF, Mg and Ti (TLD-100) Reproducibilit. *J Biomed Phys Eng*, 2015.

[48] M.G. Sabini, L. Raffaele, M. Bucciolini, G.A.P. Cirrone, G. Cuttone, S. Lo Nigro, S. Mazzochi, V. Salamone, and L.M. Valastro. The use of thermoluminescent detectors for measurements of proton dose distribution. *Radiation Protection Dosimetry*, 101:453–456, 2002.